Polyampholyte Hydrogels for Tissue Engineering and Drug Delivery Applications

A Thesis
Presented in Partial Fulfillment of the Requirements for the
Degree of Master of Science
with a
Major in Chemical Engineering
in the
College of Graduate Studies
University of Idaho
by
Emily M. Mariner

Major Professor: Matthew Bernards, Ph.D.
Committee Members: Nathan Schiele, Ph.D.; Mark Roll, Ph.D.
Department Administrator: Eric Aston, Ph.D.

May 2019

Authorization to Submit Thesis

This Thesis of Emily M. Mariner, submitted for the degree of Master of Science with a Major in Chemical Engineering and titled "Polyampholyte Hydrogels for Tissue Engineering and Drug Delivery Applications" has been reviewed in final form. Permission, as indicated by the signatures and dates below, is now granted to submit final copies to the College of Graduate Studies for approval.

Major Professor: _____ Date: _____
Matthew Bernards, Ph.D.

Committee Members: _____ Date: _____
Nathan Schiele, Ph.D.

_____ Date: _____
Mark Roll, Ph.D.

Department Administrator: _____ Date: _____
Eric Aston, Ph.D.

Abstract

Polyampholyte polymers are being investigated for biomedical applications such as drug delivery and tissue engineering. These polymers are composed of equimolar positively and negatively charged monomers and they possess nonfouling properties that reduce the risk of a foreign body response. Nonfouling combined with tunable mechanical and drug release properties make them very suitable for many applications in the biomedical field.

In this work, the mechanical and degradation properties are characterized as a function of cross-linker species. Specifically, we evaluated the influence that the number of ethylene glycol repeat units has on the overall material performance by synthesizing and evaluating hydrogels containing di-, tri-, and tetra-ethylene glycol dimethacrylate cross-linker species. The degradation studies were conducted for over 100 days in Sorenson's buffer with pH values of 4.5, 7.4, and 9.0 by tracking the swelling behavior and weight change over time. The mechanical properties were evaluated using compression and tensile testing to failure.

Additionally, a piezoelectric droplet on demand generator was designed and constructed to produce polyampholyte microspheres for drug delivery. The microspheres were composed of a 1:1 molar ratio of [2-(acryloyloxy)ethyl] trimethylammonium chloride (TMA, positively charged) and 2-carboxyethyl acrylate (CAA, negatively charged) monomers cross-linked with TEGDMA. Polymerization was initiated using LAP photoinitiator upon droplet ejection. This study evaluated the viability of using these microspheres for releasing vitamin D_3 and metanil yellow into biological media. The size and nonfouling properties were also investigated.

In these studies, we found that the cross-linker chain length does influence the mechanical properties and degradation behavior. Droplet generation of nonfouling polyampholyte microspheres was successful; however, there was no success with long-term drug release of vitamin D_3 or metanil yellow. Polyampholytes still show promise for use in biomedical applications, though the droplet generator would need some modifications to use these microspheres for drug delivery.

Acknowledgements

I would first like to thank my committee members. Dr. Matthew Bernards helped me not only with my research projects, but also helped me develop my oral and written communication skills. Dr. Nathan Schiele allowed me to use his lab for tension testing and improved my understanding of tissue engineering and biomechanics. Dr. Mark Roll provided me with more knowledge on polymers and polymer chemistry. I would also like to thank my fellow researchers. Stephanie Haag assisted me with all of the tensile testing and Jackie Martinez helped me with my drug release studies. Finally, I would like to thank some of the faculty and staff who helped make my research here possible, including Gail Bergman and Margaret Baker. Dave MacPherson assisted me with all of the electronics on my droplet generator as well as helped me troubleshoot emergent issues. Charles Cornwall built my generator and when he was not available, Brian Petty was always there to help. Dr. Indrajit Charit allowed me access to his Instron so I could complete all of my compression testing.

The Congressionally Directed Medical Research Program, Discovery Award, Grant #W81XWH-15-1-0664 and the NASA Idaho Space Grant Consortium, funded this research.

Dedication

I would like to thank my very best friend, Jacob Bryan for giving me so much love and support during my time here as a graduate student. Moreover, I would not have been able to do this without my friends and family, so I would like to thank my parents, Jerry and Denise Mariner, and my siblings Sidney and Craig Mariner. Finally, I would like to acknowledge all of my friends who supported me and encouraged during my graduate studies.

Table of Contents

List of Tables

List of Figures

Statement of Contribution

In this work, I have included a submitted paper, “Impacts of Cross-Linker Chain Length on the Physical Properties of Polyampholyte Hydrogels” with another author, Stephanie Haag. Her contribution to this work was completing all of the tension tests, while I completed the compression, protein conjugation, nonfouling, degradation studies, and data analysis.

Chapter 1: Introduction

Polymeric materials are being looked at for a number of biomedical applications, including tissue engineering and drug delivery. In the biomedical field, there is a need for engineered scaffold materials that can improve and facilitate wound healing in severely damaged tissues. These scaffolds must have several important properties to ensure successful tissue recovery. First, the biomaterial must be nonfouling, or resistant to nonspecific protein adsorption. It is hypothesized this feature will minimize any foreign body response, preventing connective tissue from becoming inflamed and scarred [1, 2]. Inflammation and scarring leads to encapsulation of the implanted biomaterial, preventing the biomaterial from fully integrating and maintaining functionality [3, 4]. Second, the biomaterial must also facilitate cell adhesion, migration, and remodeling to promote tissue regeneration [5]. To do this, the material must present biochemical cues specific to the target tissue. Third, the scaffold material should be biodegradable and not break down into components that are toxic or harmful to the surrounding cells and tissues [6, 7]. Ideally, the material will break down at the same rate at which tissue is reforming to prevent defects in the regenerating tissue [1, 8]. Finally, an implant must have mechanical properties similar to the tissue it will be integrated with, to allow for faster return to functionality [6, 7, 9]. Mechanical properties also impact the differentiation of seeded or recruited stem cells, which is important for the regeneration of the intended tissue [10, 11].

These characteristics are also important for drug delivery vehicles for many of the same reasons. Tailorable physical properties are also very important in order to achieve controlled release rates based on pore size, swelling properties, and degradation rate [1, 12]. There is a need for drug delivery systems with controlled release rates for better efficiency and for the ease of the patient [13]. Extended release reduces the dosing frequency, extends the therapeutic level of drug concentration, and reduces risk of potential toxic concentrations of the drug during release [12-16].

There have been many approaches to develop engineered biomaterials to fulfill these criteria, but it has been difficult to design something that incorporates all of these properties. Hydrogels are the standard for tissue engineering because of their high water content and general biocompatibility [1, 17, 18]. They also have tunable properties and the ability to be synthesized on a larger scale [1, 5]. Some common chemistries that have been explored for tissue engineering include poly(lactic acid) (PLA), poly(hydroxyethyl methacrylate) (PHEMA), and poly(caprolactone) (PCL) [1, 19]. PLA is biologically inert and has high degradability [18, 20]. However, this material still invokes an inflammatory response, as it is not nonfouling [20, 21]. Additionally, its degradation rate is relatively slow [21]. PHEMA has been used in tissue engineering for decades because it is biocompatible and has some ability to reduce nonspecific protein adsorption [19]. Since this material is only low fouling,

it still causes inflammation when implanted. While PCL is biodegradable and inexpensive, it is hydrophobic and has poor cytocompatibility [22, 23].

Another common material is polyethylene glycol (PEG), which is resistant to nonspecific protein adsorption leading to its widespread use in biomedical systems. PEG based materials are known to oxidize *in vivo* [24]. This ultimately leads to protein adsorption and cell attachment as it breaks down into acids and aldehydes [24]. It has also been reported that humans have developed antibodies to PEG, suggesting there is a need to find alternative biomaterials [25, 26].

Zwitterionic materials have recently become of interest for biomedical applications because they have shown great antifouling properties when compared to other nonfouling materials such as PEG [27, 28]. These neutral systems are composed of mixed charged functional groups throughout the polymer. As a result, they are extremely hydrophilic due to the large number of charged regions [25]. The most widely studied zwitterionic materials are polycarboxybetaine (pCB), polysulfobetaine, and polyphosphorylcholine [25, 27]. pCB-based materials in particular, have gained a lot of attention because of their superior antifouling properties, biocompatibility, and functionalization capabilities [25, 27, 29]. Functionalization allows for the covalent attachment of biomolecules and pCB is highly functionalizable due to its many carboxyl groups [29, 30]. However, one limitation of zwitterionic polymers is that their physical properties are dependent on the underlying monomer, making their physical properties less tunable than other materials [31].

One family of materials that presents many of the desired properties for tissue engineering and drug delivery are polyampholyte hydrogels, which are a subclass of zwitterionic polymers. They are being considered for tissue engineering and drug delivery applications due to their unique characteristics including nonfouling properties, ability to deliver biomolecules to the body, and tunable mechanical properties [32, 33]. Polyampholyte hydrogels are composed of mixtures of positively and negatively charged monomer subunits, resulting in an overall neutral charge [34]. The nonfouling properties are likely derived from the formation of a strong hydration layer [33, 35-37]. Polyampholyte hydrogels have tunable mechanical properties depending on both the underlying of monomer composition and the cross-linker density [33, 36]. It is hypothesized that the tunable mechanical and physical properties of these polyampholyte hydrogels make them a suitable platform for biomedical applications. This hypothesis was tested in two separate studies, one looking at how cross-linker chain length effects the mechanical properties and degradation behavior. The second, developing polyampholyte microspheres for drug delivery using a droplet on demand generator. Each of these studies are discussed in further detail in Chapters 2 and 3, respectively.

Chapter 2: Impacts of Cross-Linker Chain Length on the Physical Properties of Polyampholyte Hydrogels

Introduction

Polymeric tissue engineering scaffolds have shown promise to aid in regeneration and repair of damaged tissue. In particular, nonfouling polymers have been proposed for eliminating biomaterial-induced concerns such as infection, scarring, and rejection by the immune system. Polyampholyte polymers are one class of nonfouling polymers that are composed of an equimolar mixture of positively and negatively charged monomer subunits. They possess nonfouling properties, bioactive molecule conjugation, and tunable mechanical properties [33]. While several beneficial features of polyampholytes have been demonstrated, their degradation behaviors are relatively unknown. Understanding the degradation behavior will provide insight into the *in vivo* behavior of these materials, allowing for targeted applications in tissue engineering. Additionally, mechanically testing has not been performed with different cross-linkers for these TMA/CAA hydrogels.

It was hypothesized that different ethylene glycol chain lengths will lead to variation in the physical and mechanical properties, without impacting the multifunctional nonfouling capability. Therefore, the goal of this investigation is to characterize the degradation and physical properties of polyampholytes with different ethylene glycol cross-linkers. The polyampholytes used in this study contained equimolar amounts of cationic [2-(acryloyloxy)ethyl] trimethylammonium chloride (TMA) and anionic 2-carboxyethyl acrylate (CAA) monomers, which are shown in Figure 2-1. Hydrogels were synthesized with one of three chemical cross-linkers, di-, tri-, or tetra-ethylene glycol dimethacrylate (DEGDMA, TEGDMA, and Tetra-EGDMA), also shown in Figure 2-1, to study how the cross-linker chain length impacts the properties of polyampholyte hydrogels. The conjugation capabilities and nonfouling were validated using fluorescently labeled bovine serum albumin (FITC-BSA) and microscopy to verify the key multifunctional capabilities were not affected by cross-linker chain length. The compressive and tensile properties were quantified, and the degradation behavior as a function of pH was determined. The degradation studies were conducted for over 100 days in Sorenson's buffer with pH values of 4.5, 7.4, and 9.0 by tracking the swelling behavior and weight change over time. The mechanical properties were assessed using compression and tensile testing to failure. The results demonstrate the tunability of both the degradation behavior and mechanical properties through the cross-linker selection, without impacting the underlying nonfouling and biomolecule delivery capabilities. Therefore, it is concluded that polyampholyte hydrogels represent a promising tunable platform for tissue engineering.

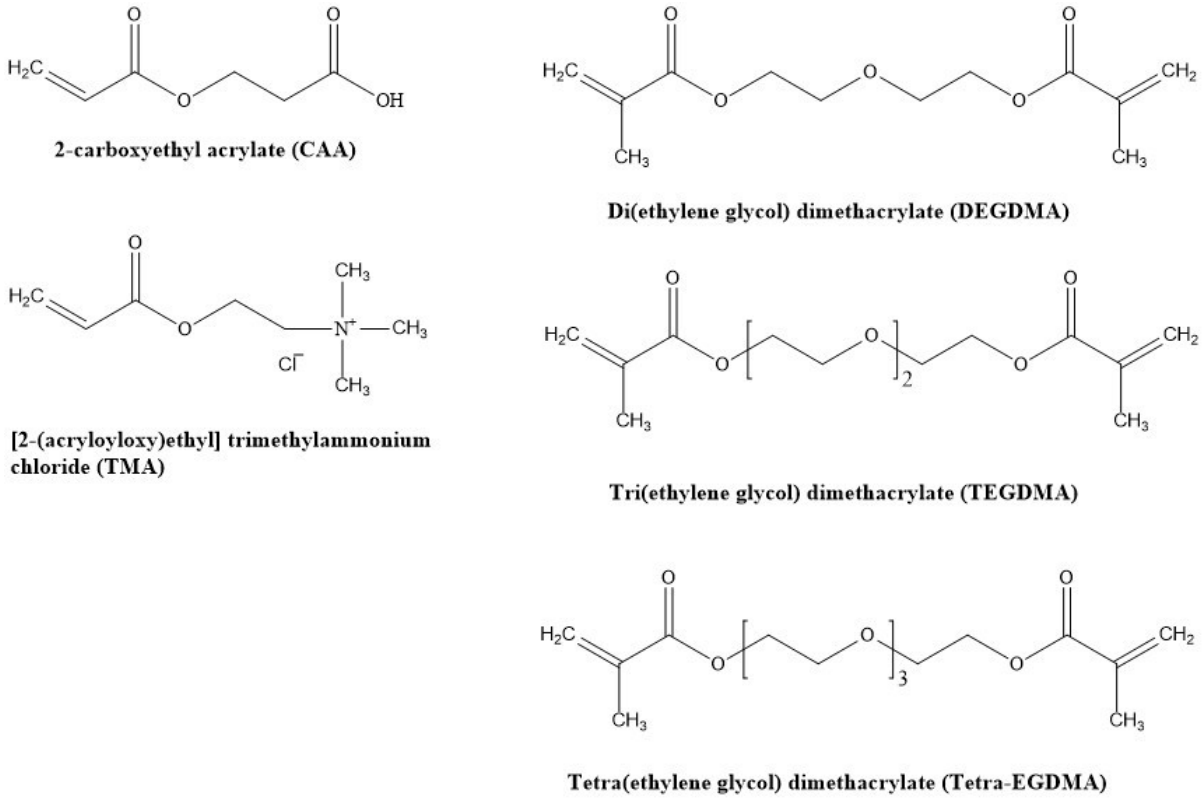

Figure 2-1 Chemical structures of the monomers and cross-linkers used in this study.

Methods and Materials

Materials

Ethylene glycol, phosphate-buffered saline (PBS, pH 7.4), fluorescein isothiocyanate bovine serum albumin (FITC-BSA), TMA, CAA, TEGDMA, DEGDMA, Tetra-EGDMA, sodium hydroxide, ammonium persulfate (APS), sodium metabisulfate (SMS), N-(3-dimethylaminopropyl)-N'-ethylcarbodiimide hydrochloride (EDC), and N-hydroxysuccinimide (NHS) were purchased from Sigma-Aldrich. Potassium phosphate monobasic and sodium phosphate dibasic, anhydrous were purchased from VWR. Ethanol was purchased from Greenfield Global. All chemicals were used as received.

Hydrogel Synthesis

Hydrogels were synthesized using equimolar concentrations of TMA and CAA using procedures described previously [33]. In short, 2 mL of a buffer solution containing 3 M NaOH, ethanol, and ethylene glycol in a 1.5:1:1.5 volume ratio was mixed with 4 mmol of TMA and CAA each and mixed thoroughly. One of the three cross-linkers was added in with monomer to cross-linker ratios of 26.3:1 (1X), 13.2:1 (2X), or 6.6:1 (4X). The reaction was initiated by adding 32 µL of 40% w/w APS and 32 µL of 15% w/w SMS and the solution was then transferred into a polytetrafluoroethylene (PTFE) mold. The hydrogels polymerized at room temperature for 24 hours. With the exception of degradation, all hydrogels were then soaked for 24 hours in PBS and used in subsequent studies.

Nonfouling and Protein Conjugation

For nonfouling and conjugation testing, hydrogels were synthesized in a flat plate mold formed from two microscope slides clamped around a 1/8” PTFE spacer. Following synthesis, the hydrogels were soaked in PBS for 24 hours and then they were punched with a 5mm biopsy punch [33]. Conjugation and control samples were first soaked in a solution of 0.05 M NHS and 0.2 M EDC for 7 minutes, while the nonfouling samples were soaked in neutral PBS. The nonfouling and conjugation samples were then exposed to 10 µL of 1 mg/mL FITC-BSA in PBS for 15 minutes, while the control samples were soaked in neutral PBS. Finally, all samples were soaked in 1 mL of NaCl-PBS with a pH of 9.0 for 30 minutes, followed by 1 mL neutral PBS for 40 minutes. Nonfouling and conjugation were evaluated by comparing the fluorescence of these samples to the control sample using an inverted fluorescent Nikon microscope with a 4X objective. Images were captured using NIS Elements imaging software.

Compression Testing

For compression testing, hydrogels were synthesized in a cylindrical PTFE mold with a 5/8" inner diameter. Compression samples were made by tripling the above procedures. After the samples soaked for 24 hours in PBS, they were cut using a razor and mold to obtain 10 mm tall hydrogel cylinders. Compression tests were conducted using an Instron equipped with a 100 kN load cell. Samples were compressed until they shattered at a rate of 0.1 mm/s. The maximum stress and strain were obtained from the force displacement curve and the Young's modulus was taken from the linear region (75-85% of the maximum strain) of the stress-strain curve.

Tensile Testing

For tensile testing, hydrogels were synthesized in a PTFE dog-bone shaped mold. Tensile testing was conducted using a custom tensile load frame and a 150 g load cell [38]. Samples were stretched at a rate of 0.1 mm/s until fractured. The maximum stress and strain were obtained from the force displacement curve and the Young's modulus was taken from the linear region (50-100% of the maximum strain) and toe region (0-0.1 strain values) of the stress-strain curve.

Degradation Studies

For degradation testing, hydrogels were synthesized in the flat plate mold described above. After polymerizing for 24 hours, samples were immediately cut into 1 cm squares and placed in individual 50 mL centrifuge tubes containing Sorenson's buffer. Sorenson's buffer with pH values 4.5, 7.4, and 9.0 were used to induce degradation under different conditions. Degradations studies were conducted over a period of 113 days with 1X cross-linker density hydrogels. At each measurement time point, the samples were removed from the buffer and characterized before being placed in fresh buffer. Wet weight was measured using a scale and swelling measurements were taken using calipers.

Data Analysis

All results are presented as the average ± standard deviation from the evaluation of three samples replicated three independent times (n=9). Statistical significance was evaluated using a one-way analysis of variance (ANOVA) at a 95% confidence interval ($p < 0.05$) using OriginPro 2017 (OriginLab Corporation, MA).

Results

Nonfouling and Protein Conjugation

Polyampholyte hydrogels are of interest for tissue engineering applications because of their demonstrated multifunctionality [33]. Therefore, it was important to verify that the additional cross-linker species investigated in this study did not impact their previously demonstrated nonfouling and conjugation capabilities. Non-specific adsorption of FITC-BSA was used to verify the nonfouling properties using fluorescent microscopy. Figures 2-2 a-c show representative images of TMA:CAA hydrogels following exposure to FITC-BSA and control hydrogels that have not been exposed to any protein. There are minimal to no differences in the fluorescence between these samples. Therefore, the results suggest that the nonfouling properties are not impacted by the different cross-linker species. The protein conjugation capabilities were also verified with FITC-BSA and fluorescent microscopy. The results can be seen in Figures 2-2 d-f. These images show hydrogels with conjugated FITC-BSA adjacent to control samples. FITC-BSA conjugated samples showed bright fluorescence compared to the unexposed control group, indicating that the FITC-BSA is successfully conjugated to the hydrogels, again demonstrating that the known conjugation capabilities are not impacted by the variation in cross-linker species.

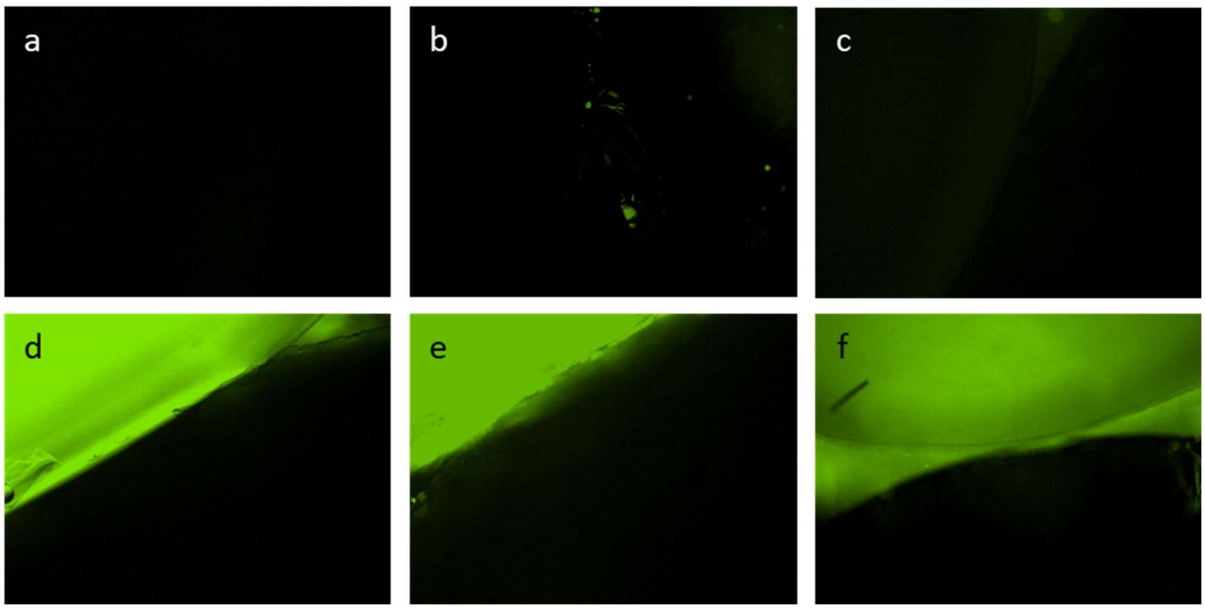

Figure 2-2 Representative fluorescent microscopy images of FITC-BSA a, b, c) adsorption and d, e, f) conjugation to TMA:CAA hydrogels with 1X cross-linker densities of a, d) DEGDMA, b, e) TEGDMA, and c, f) Tetra-EGDMA cross-linkers. Control samples are included in the bottom right of each image and they were not exposed to FITC-BSA.

Compressive Strength

The physical properties under compression were evaluated next, to identify impacts of the cross-linker length and density. Figure 2-3 a-c shows representative stress-strain curves for 1X, 2X, and 4X cross-linker density hydrogels with each cross-linker species, respectively. It can be seen that decreasing the cross-linker chain length increases both stress and strain at failure. The quantitative analysis of multiple samples, in Figure 2-3 d, show that increased cross-linker density improves the stress at failure for all the cross-linker species, as expected [33].

The maximum stress at failure value across all samples was found for the 4X cross-linker density DEGDMA hydrogels with an average stress of 863 ± 137 kPa. This value was statistically greater than the max stress at failure for both 4X cross-linker density TEGDMA and Tetra-EGDMA samples. At the 1X cross-linker density, DEGDMA samples had the statistically lowest fracture stress. DEGDMA samples also demonstrated the largest impact as cross-linker density was increased, as they had the greatest max stress at a 4X cross-linker density. The only statistically significant difference in the 2X cross-linker density samples was seen between the TEGDMA and Tetra-EGDMA results, with TEGDMA samples having a higher stress at failure. The maximum strain at failure results are shown in Figure 2-3 e. Only the Tetra-EGDMA samples showed significant variation in the max strain at failure as a function of cross-linker density, with a statistically significant drop between the 1X and 4X cross-linker density samples. Across all cross-linker densities, DEGDMA samples presented the highest max strain at failure, with the greatest average strain of 0.51 ± 0.04 for the 2X cross-linker density, but this value was not statistically significant from the 1X and 4X DEGDMA density results. At the 4X cross-linker density there were statistically significant differences between all of the cross-linker species. The results indicate that increasing cross-linker chain length decreases the compressive strain at failure. Finally, the elastic moduli of the various samples were evaluated, and these results are shown in Figure 2-3 f. For the most part, the cross-linker species did not impact the elastic modulus under compression. The modulus increased uniformly across the cross-linker species with increasing cross-linker density and the maximum elastic modulus was seen for 4X density DEGDMA samples with a value of 3298 ± 825 kPa.

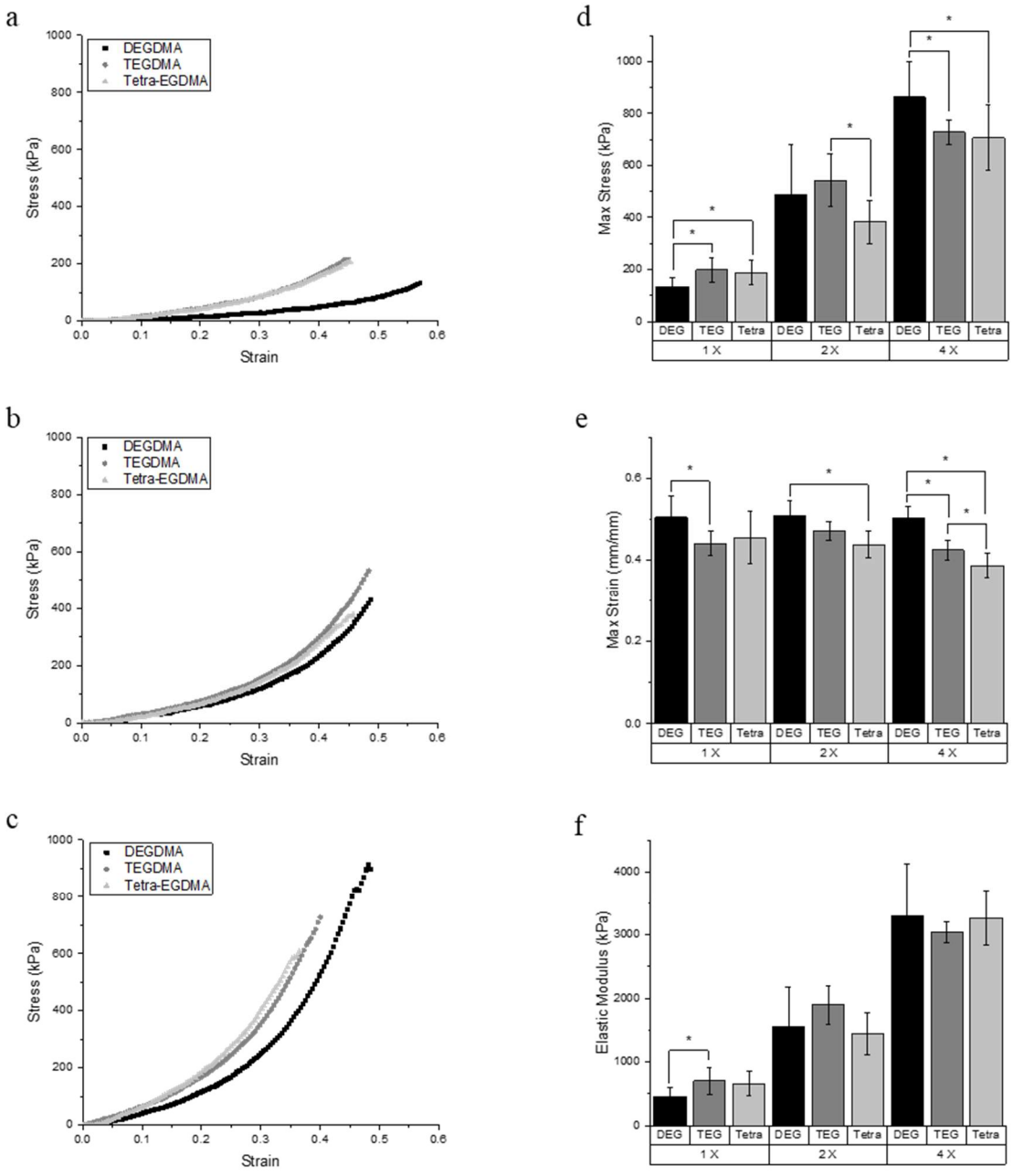

Figure 2-3 Compressive properties of hydrogels with different cross-linker species and densities. a, b, and c) Representative stress-strain curves for 1X, 2X, and 4X cross-linker density hydrogels, respectively, d) maximum stress at failure, e) maximum strain at failure, and f) elastic modulus taken from the linear region. A * indicates a statistically significant difference at a 95% confidence interval ($p < 0.05$) between the samples identified.

Tensile Strength

The physical properties under tension were evaluated, again to identify the influence of the cross-linker species and density. The tensile properties of this family of materials have not previously been tested. Figure 2-4 a-c shows representative stress-strain curves for 1X, 2X, and 4X cross-linker density hydrogels in tension, respectively. Each curve for the 4X cross-linker density presents a different profile with a low strain transition region seen with the Tetra-EGDMA hydrogel curves (~18% of total strain), no transition region with the TEGDMA hydrogels, and a mid strain transition region in the DEGDMA hydrogel curves (~56% of the total strain). The TEGDMA hydrogel curves have a nearly linear stress-strain curve at a 4X cross-linker density, while the 1X and 2X cross-linker density curves have profiles similar to DEGDMA. The slope of Tetra-EGDMA stress-strain curve is similar to that of TEGDMA after the inflection region, while the slope of the DEGDMA stress-strain curve is similar to TEGDMA before its transition region.

The results in Figure 2-4 d indicate that the fracture stress at failure increases with increasing cross-linker density, again as expected. However, in contrast to the compressive fracture behaviors, Tetra-EGDMA demonstrates the highest values, reaching a maximum tensile fracture stress of 58.1 ± 13.8 kPa for the 4X cross-linker density hydrogels. Tetra-EGDMA also has the largest change as the cross-linker density is increased. Unlike the compression study, the fracture strain decreased with increased cross-linker density. A much more significant change was seen for all three cross-linkers species as the cross-linker concentration increased. As before, there was little significance between the strain values as a function of cross-linker species, at a given cross-linker density, though DEGDMA had a greater strain value under all conditions. Finally, Figure 2-4 f shows the average elastic modulus for these samples under tension in both the toe region (solid) and linear region (patterned). The elastic modulus was greater in the toe region than it was in the linear region and the overall elastic modulus increases with increasing cross-linker density. As with the maximum stress under tension data, the Tetra-EGDMA samples have the highest elastic modulus values and show the largest dependence on cross-linker density.

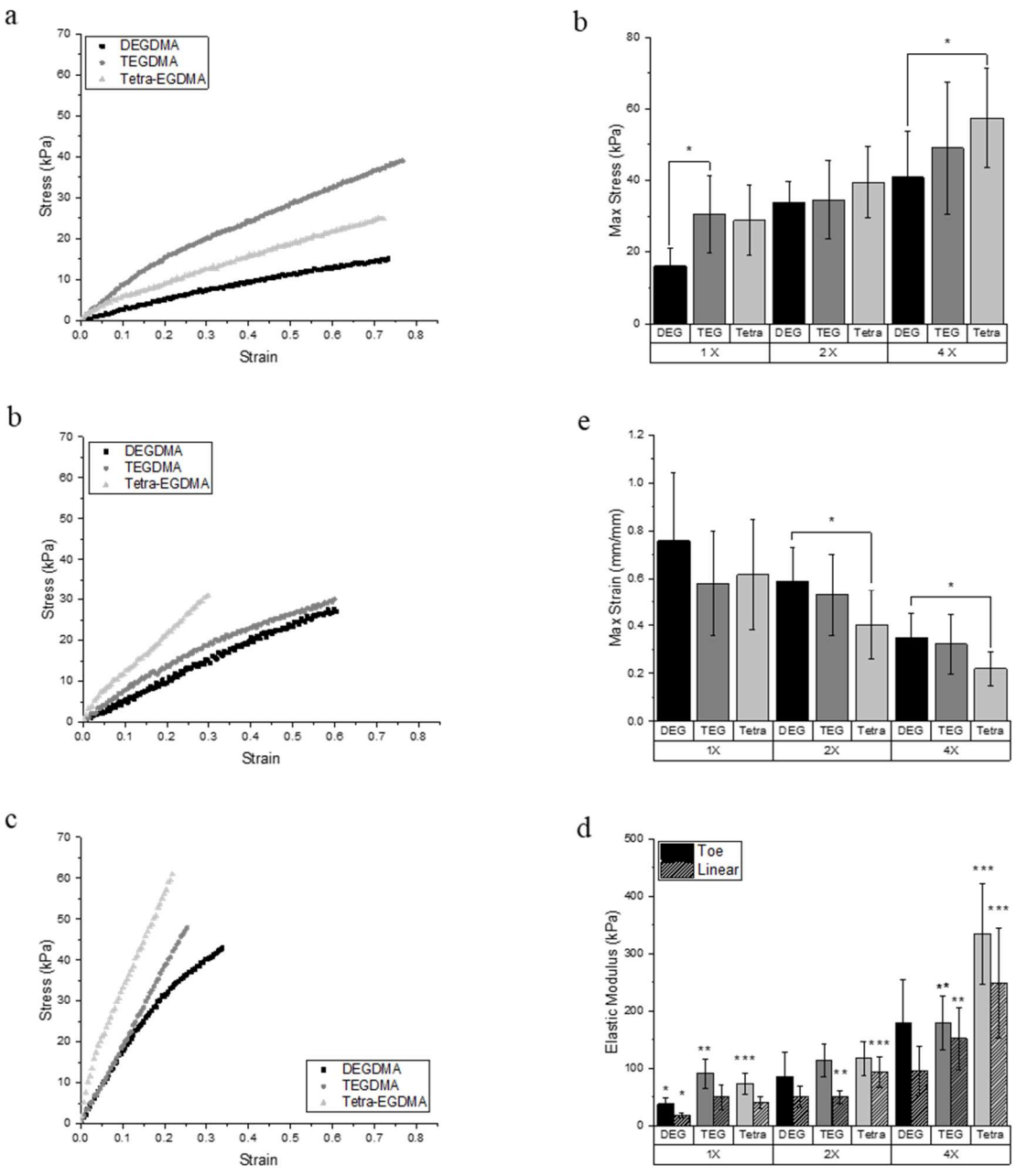

Figure 2-4 Tensile properties of hydrogels with different cross-linker species and densities. a, b, and c) Representative stress-strain curves for 1X, 2X, and 4X cross-linker density hydrogels, respectively, d) maximum stress at failure, e) maximum strain at failure, and f) elastic modulus taken from the toe (solid) and linear (patterned) regions. A * indicates a statistically significant difference between the samples identified at a 95% confidence interval ($p < 0.05$). For the modulus, a *, **, and *** indicates a statistically significant difference for the results between the DEGDMA and TEGDMA samples, the TEGDMA and Tetra-EGDMA samples, and the DEGDMA and Tetra-EGDMA samples, respectively, all at a 95% confidence interval ($p < 0.05$).

The magnitude of change relative to the 1X cross-linker density was evaluated to look for trends between the different species. The magnitude of change for each cross-linker species as cross-linker density was increased was very different and is demonstrated in Figure 2-5. It can be seen that the change is not necessarily correlated to the amount of additional cross-linker, but depends more on the cross-linker species. For compression samples, DEGDMA shows the most drastic change as the cross-linker density increases for stress and modulus. TEGDMA shows the least amount of change in both compression and tension. It should also be noted that DEGDMA and Tetra-EGDMA present similar changes under tension as cross-linker density increases, whereas TEGDMA shows little change. Figure 2-5 further illustrates that there is not much change in compressive strain as the cross-linker density changes.

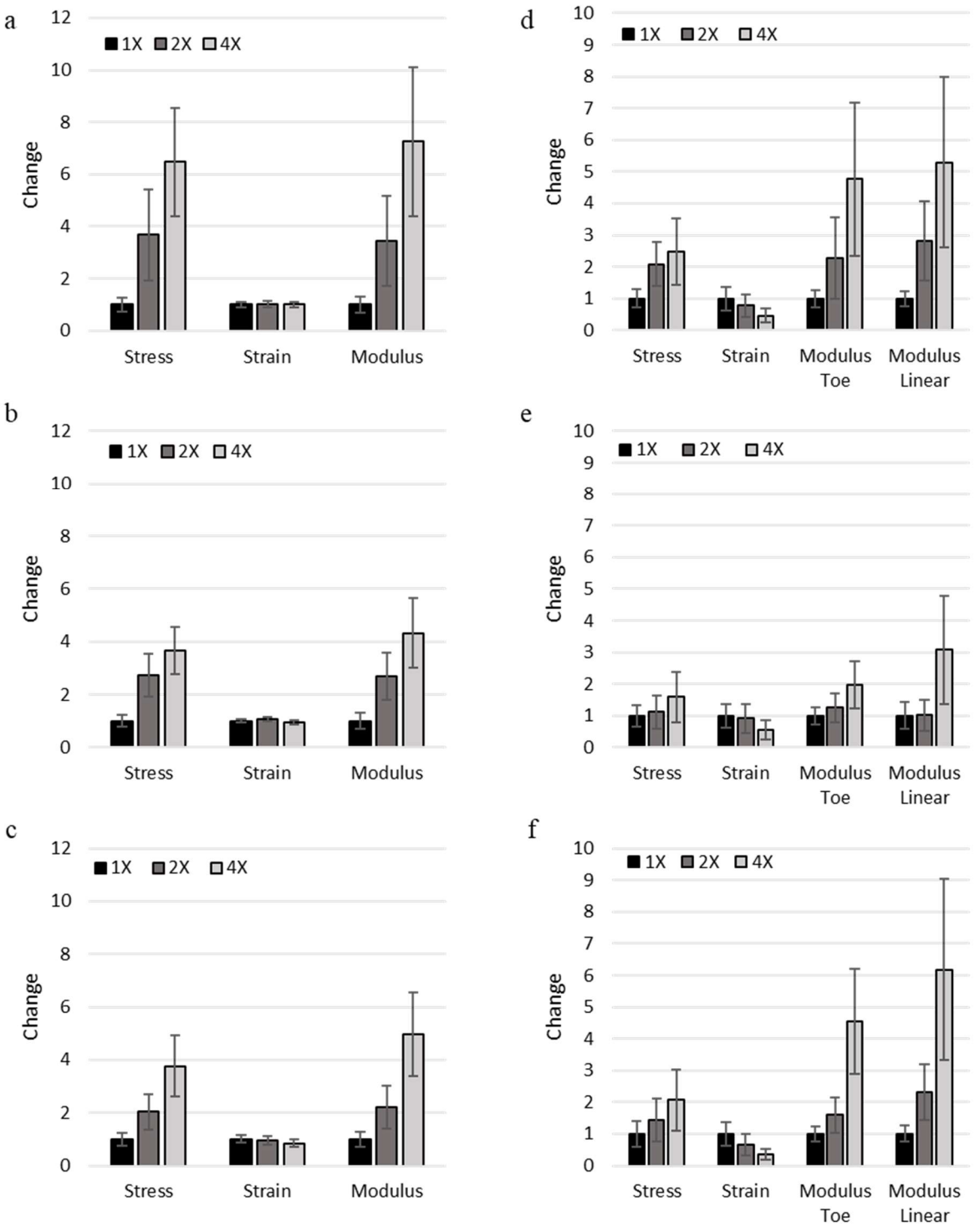

Figure 2-5 Change in magnitude of stress, strain, and modulus for each cross-linker species in compression and tension for a, d) DEGDMA, b, e) TEGDMA, and c, f) Tetra-EGDMA as normalized to the 1X cross-linker density, respectively.

Degradation Studies.

The degradation behaviors of TMA/CAA polyampholyte hydrogels have not been characterized previously. For this degradation study, 1X cross-linker density hydrogels with the three different cross-linkers species were monitored for 113 days in Sorenson's buffer with acidic (4.5), neutral (7.4), and basic (9.0) pH conditions. The degradation was monitored by tracking the sample swelling and weight changes over time and the results are summarized in Figure 2-6. There were insignificant changes in the swelling and weight change behavior for all three cross-linker species under the neutral and basic conditions, over the time period evaluated here. Degradation occurred in the acidic environment for all three cross-linker species, ultimately leading to full sample breakdown after ~110 days for Tetra-EGDMA cross-linked samples. The Tetra-EGDMA hydrogels increased in both weight and swelling over time. Conversely, the DEGDMA and TEGDMA cross-linked hydrogels decreased in both size and weight. They also did not reach full degradation like the Tetra-EGDMA hydrogels over the time period evaluated. These paired results suggest that the Tetra-EGDMA samples degraded via bulk degradation pathways, while the DEGDMA and TEGDMA degraded via surface degradation pathways, as discussed in more detail below.

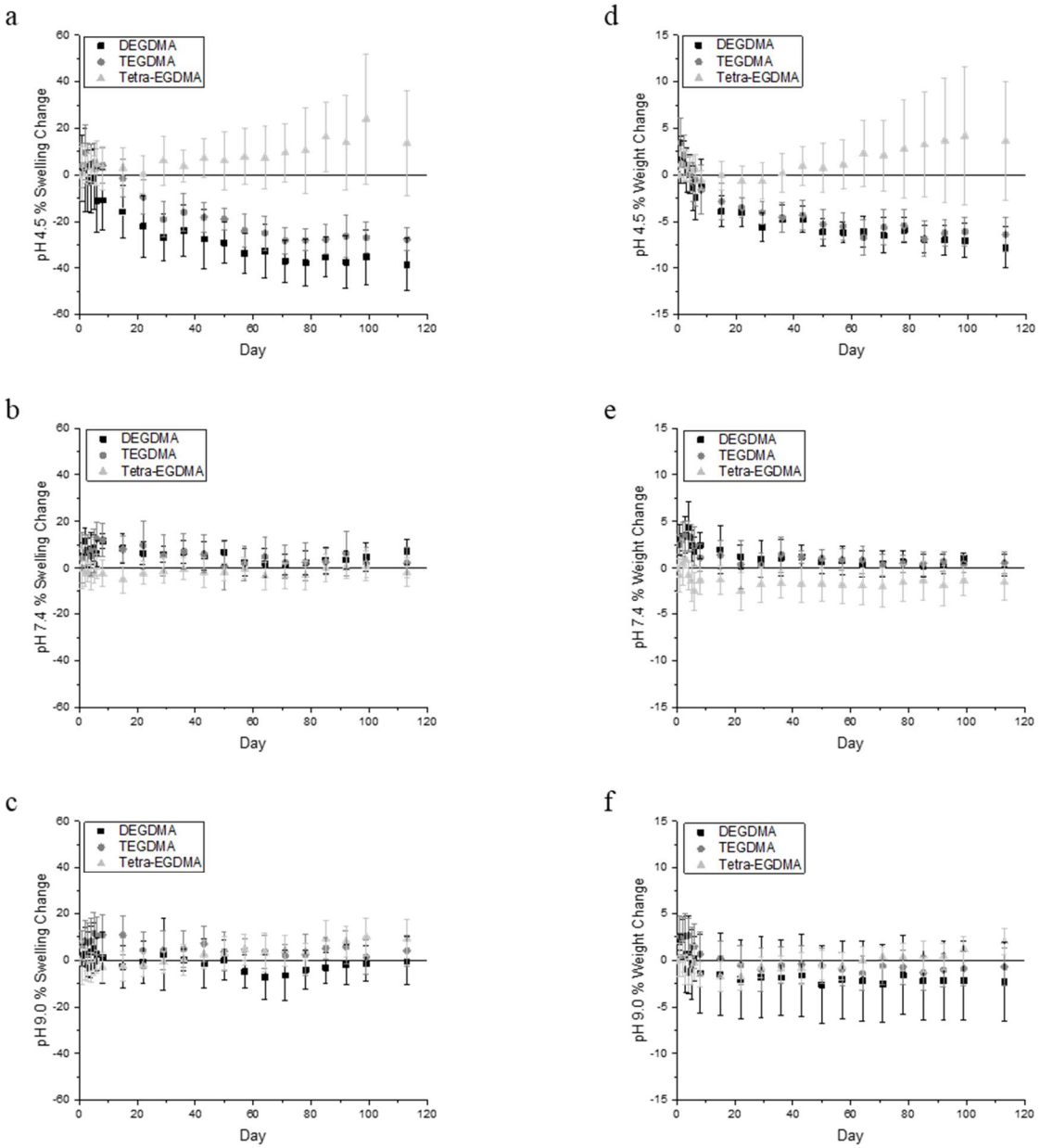

Figure 2-6 Mean ± standard deviation of the percent change in a, b, c) swelling and d, e, f) weight for 1X cross-linker density hydrogels in a, d) acidic, b, c) neutral, and c, f) basic pH conditions.

Discussion

The compression samples show that increasing the cross-linker density generally leads to increasing stress at failure and elastic modulus, which has been seen in previous studies [36, 39]. Specifically, the physical properties under compression for TMA/CAA hydrogels with a TEGDMA cross-linker have been tested previously and the trends between the previous results and this study are similar [33]. The results in this study show that the available range of mechanical properties can be expanded even further by varying the length of the cross-linker species, suggesting a wider range of tunability. A similar range is also demonstrated under tension in this study as well.

The results on Figure 2-3 e show that increasing the cross-linker chain length decreased the compressive strain at failure specifically at higher cross-linker densities. Additionally, there were no significant differences in strain for each cross-linker species with changes in the cross-linker density. This indicates that the compressive strain is not dependent on the amount of cross-linker in the hydrogel. These hydrogels are made up of 90% water and has been demonstrated that changing the cross-linker density does not change the hydration level [33]. This high water content leads to bulk incompressible behavior, as water is generally treated in this fashion. Therefore, there is no change in strain as a function of cross-linker density.

When the 4X cross-linker density stress-strain curves under tension are examined (Figure 2-4 c), it is evident that all three cross-linker species have a portion of the curve that has similar slope with each other. This occurs before the transition region in the DEGDMA cross-linked samples, across the entirety of the profile for the TEGDMA cross-linked samples, and after the transition region in the Tetra-EGDMA cross-linked samples. After the transition region, the system has very similar behavior to the TEGDMA samples. While similar trends exist in the 1X and 2X cross-linker density stress-strain curves, they are not as prevalent because the pendant group packing densities are lower. Polymers have a coiled structure and the stress-strain profiles seen in Figure 2-4 a and b are typical for rubber like materials. As the hydrogels are pulled, the polymer chains rearrange and straighten out. Polymers act as an entropic spring, and the change in modulus is a result of that. At the coiled state, they have higher entropy and that decreases as they are stretched out. As the cross-linker density is increased to 4X, the stress-strain behavior appears to transition more to a brittle plastic-like profile. This is understandable as there are more cross-links present and increased structure rigidity.

Figure 2-7 presents an example of the most tightly packed pendant group alignment; it is readily acknowledged that the pendant groups will rotate around the polymer backbone in three-dimensions to reduce the overlap and resulting steric hindrance. These polymers are also mostly made up of water, which is not apparent in this schematic. It is estimated that there are approximately 630 -

675 water molecules per each 4X cross-linker density grouping (6.6:1 monomers:cross-linker) depending on the cross-linker species. This is based on the published weight percent hydration for similar hydrogels [33]. Furthermore, as the cross-linker density is increased, it will reduce the degrees of freedom available for this pendant group rotation. This results in more overlap between pendant groups in hydrogels cross-linked with DEGDMA, which will not be seen in the TEGDMA and Tetra-EGDMA cross-linked systems.

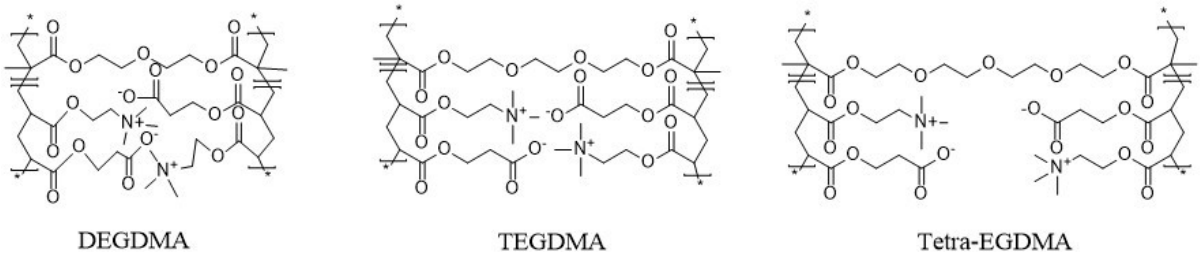

Figure 2-7 Schematic showing the packing density of the pendent side chains with a) DEGDMA, b) TEGDMA, and c) Tetra-EGDMA cross-linkers.

The packing density theory can be used to explain the degradation study results. The Tetra-EGDMA cross-linked hydrogels present a different degradation behavior than the DEGDMA and TEGDMA cross-linked hydrogels under acidic conditions. All of the hydrogels degrade via acid hydrolysis of the ester groups present in both the cross-linkers and monomers [1, 6]. The results indicate that the DEGDMA and TEGDMA cross-linked hydrogels degrade via surface degradation pathways (shrinkage and weight loss), while the Tetra-EDGMA hydrogels degrade via bulk degradation pathways (swelling and weight gain) [40, 41]. The strong electrostatic interactions that occur between adjacent polymer chains cross-linked with either DEGDMA or TEGDMA cross-linkers provide steric hindrance that limits accessibility to the ester groups of the cross-linker where overall degradation occurs. Therefore, degradation only occurs at the surface and outmost layers of the hydrogels. In contrast, the pendant groups of adjacent polymer chains in hydrogels cross-linked with Tetra-EGDMA have wider spacing, facilitating easier penetration into the hydrogel and bulk degradation.

Conclusion

In this work, polyampholyte hydrogels were formed from equimolar mixtures of TMA and CAA charged monomer subunits with three different ethylene glycol based cross-linkers (di-, tri-, and tetra-ethylene glycol). Fluorescent microscopy evaluations confirmed that the multifunctional nonfouling and protein conjugation capabilities of TMA/CAA hydrogels were not impacted by the cross-linker species. The compression and tensile properties of this family of hydrogels were evaluated across a range of cross-linker densities and the results suggest that this is another way that polyampholytes can be tuned. The cross-linker length and subsequent packing density impact the acid hydrolysis degradation pathway for this family of hydrogels. Hydrogels cross-linked with DEGDMA and TEGDMA degraded via surface degradation pathways, while those cross-linked with Tetra-EGDMA degraded via bulk degradation pathways. Molecular dynamics investigations are on-going, and they will provide further mechanistic insight into the proposed theories. However, the results from this study clearly demonstrate the broad tunability of polyampholyte hydrogels for tissue engineering applications.

Chapter 3: Polyampholyte Microspheres for Extended Drug Delivery

Introduction

Polymer microspheres are becoming more prevalent for medical applications because they have several benefits including control of size and they are cheap to produce [12, 42]. Some common methods of creating polymer microspheres include emulsion, dispersion, and suspension, which requires the use of a surfactant to act as a stabilizer as the microspheres form [13, 42]. They can be used as drug delivery vehicles, bulking agents, and embolic particles [42]. Bulking agents are materials that can be used to replace lost volume in tissue due to aging and disease [42]. Use of microspheres as bulking agents can give structure and support to muscles that open and close tubular structures in the body [42]. For instance, bulking agents are in wide use to treat female stress urinary incontinence [42-44]. Embolic particles can be used to block blood vessels for to prevent tumor development [42]. The use of microspheres for drug delivery is of growing interest because of their ability to be tuned for specific purposes and their controllable release [12, 13, 45]. This chapter will specifically look at microspheres for drug delivery applications.

There are several important factors that control release rate, including microsphere size, pH, temperature, crystallinity, and porosity [13, 46, 47]. Larger microspheres tend to have slower release rates, whereas smaller microspheres have much faster release rates [13, 47, 48]. Size control is also important for the desired application. For example, if the microspheres are to be administered by injection, they must be under 6 μm in diameter to prevent capillaries from being blocked [13]. To reach certain organs, they sometime must be even smaller (5-100 nm) [13, 49]. Using pH as a method for controlled release could allow for targeted applications [13, 46, 50]. One example of this is to tailor the release in the gastro-intestinal tract, where there is large variability in pH [51]. It might be desired to release site-specific drugs in the stomach where the pH is between 1.5-3.5, vs the intestines where the pH varies between 5-7.5 [51, 52].

Nonfouling polymers are being considered as a drug delivery vehicle because they have the potential to allow extended drug release without the body's natural immune response clearing the drug carrier from the blood stream [53]. Polyampholyte hydrogels can potentially be used as a drug delivery platform because they have several unique characteristics. First, they are proven to be nonfouling. Several studies have demonstrated that they are resistant to nonspecific protein adsorption [32, 33]. Nonfouling is an important feature because it can prevent an immune response and clearance from the blood stream [53]. Second, they have tunable physical and mechanical properties based on

hydrogel composition [33, 36]. This is a key feature for drug delivery because it allows for things such as pore size, release rate, and degradation rate to be tailored to the drug species and application [1].

Finally, polyampholyte hydrogels can release biomolecules to the body, as demonstrated by Barcellona et al. in preliminary studies using metanil yellow, methylene blue, and caffeine [32]. They found that the environment the hydrogels were in affected the release properties of the selected pseudodrugs based on electrostatic interactions and molecule size. These properties can be tuned to tailor release rates for specific uses in biomedical applications. Barcellona et al. demonstrated short-term release by loading hydrogels with pseudodrugs, but polyampholytes can also be used for long-term release if the drugs are conjugated to the hydrogels [33, 46].

In this work, the release of vitamin D_3 was first studied. This drug was selected to address the issue that many space travelers have low concentrations of 25-hydroxyvitamin D in their blood stream after extensive time in space [54, 55]. Vitamin D has shown to have an effect on calcium metabolism and bone mineralization, and vitamin D deficiency is linked to type 1 diabetes, certain cancers, osteoporosis, and heart disease [55-57]. The low concentrations of 25-hydroxyvitamin D has led to increasing supplementation for space travelers, which not only increases the payload sent to space, but also increases the dosage frequency [54]. Therefore, it would be beneficial to develop a drug delivery vehicle with extended and controlled release properties to mitigate the need to increase supplementation.

It is hypothesized that a droplet on demand generator will be a good method for creating drug loaded polyampholyte microspheres. Ideally, the natural resistance to protein adsorption will lead to increased circulation times for polyampholyte polymer delivery vehicles, thereby maximizing the release and uptake of loaded supplements and drugs [53]. This hypothesis was tested by building a piezoelectric droplet-on-demand generator. Microdroplets composed of a 1:1 molar ratio of TMA and CAA monomers were formed, but other polymeric formulations can also be used. The monomers were cross-linked with TEGDMA fed at a 6.6:1 monomer to cross-linker ratio. The molecular structures are shown in Figure 2-1. Polymerization was induced using a photo-initiated free radical approach. Two photoinitiators were tested to determine their relative impacts on the polymerization process. The nonfouling properies of the resulting microspheres were evaluated using FITC-BSA and the microspheres size was determined using microscopy. The release properties of vitamin D_3 and metanil yellow were studied in PBS. The results demonstrated the capability of the piezoelectric droplet on demand generator for generating polyampholyte microspheres, and the challenges with using this approach for forming drug delivery systems.

Methods and Materials

Materials

Ethylene glycol, phosphate-buffered saline (PBS, pH 7.4), FITC-BSA, TMA, CAA, TEGDMA, cholecalciferol (vitamin D_3), and sodium hydroxide were purchased from Sigma-Aldrich. Ethanol was purchased from Greenfield Global. Lithium phenyl-2,4,6-trimethylbenzoylphosphinate (LAP) and 2-hydroxy-4'-(2-hydroxyethoxy)-2-methylpropiophenone (Irgacure 2959) were both purchased from VWR. All chemicals were used as received. The piezoelectric buzzer (102-1128-ND) was purchased from Digi-Key, and the H-bridge and LED lights were both purchased from Amazon.

Droplet generator

For this study, a droplet on demand generator was constructed based on work from Harris et al with several design modifications [58]. Figure 3-1 shows a schematic of the generator (excluding additional lights). It consists of a fluid reservoir (A) mounted on a translation stage that adjusts the height. The height is important because it determines the hydrostatic pressure at the outlet. If it is too high, droplets will form from gravity, and if it's too low, air will be sucked into the system and no droplets will form [58]. The reservoir feeds into the fluid chamber (B) that is topped with a piezoelectric buzzer (C). This sends a pulse through the generator and ejects a droplet through a nozzle (D). The droplets fall through a UV light fixture (E) while they are polymerized, and droplets are collected in a vessel below or in between the light fixtures. The system was built out of aluminum and nozzles with three different diameters (0.4, 0.6, and 1 mm) were custom made with stainless steel. Two light fixtures were built consisting of 9 365 nm LEDs each. The aluminum backing worked as the frame to mount the lights and as a heat sink. Each frame had three lights connected in series and the sets were connected in parallel as seen in the circuit diagram in Figure 3-2. The light intensity was measured with a Solarmeter® Model 5.0 Standard UVA+B Meter. The electrical components needed to run the piezo included an adjustable DC power supply, an H-bridge to switch the polarity of the supplied voltage, and an Arduino Uno microcontroller. The electrical system is shown in Figure 3-3. Hudson et al. wrote a program in MATLAB to run the system [59]. Several parameters could be changed while running the droplet generator including the frequency of pulsing and the voltage supplied to the piezo. The droplet generator could run with a frequency as low as 5 Hz, and upwards of 700 Hz. The range of freqencies tested were between 5 Hz and 30 Hz.

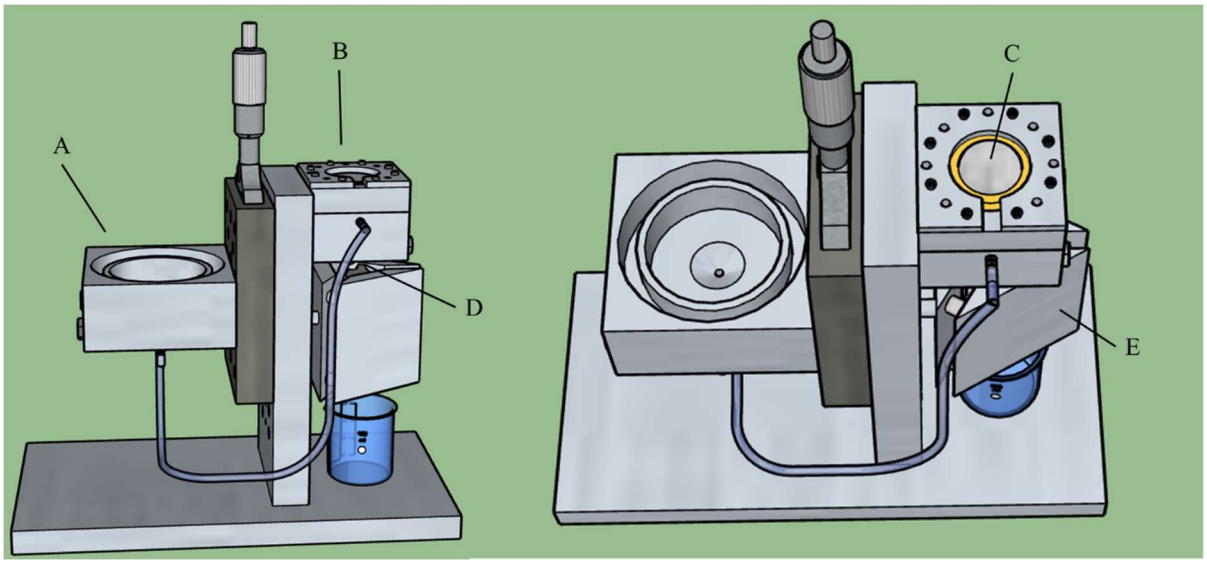

Figure 3-1 Schematic of the droplet on demand generator.

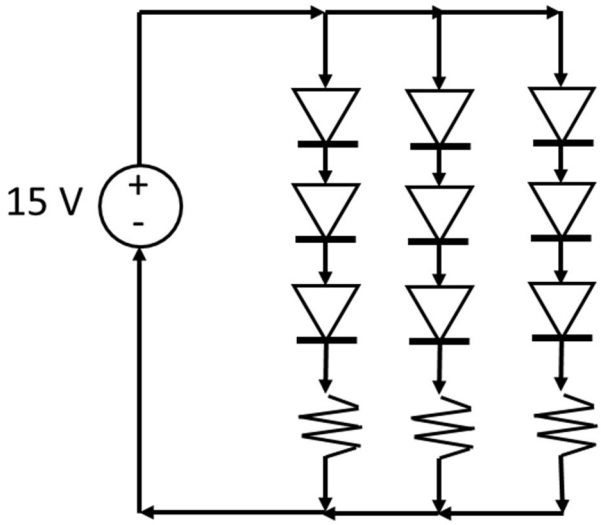

Figure 3-2 Circuit diagram for the light fixture.

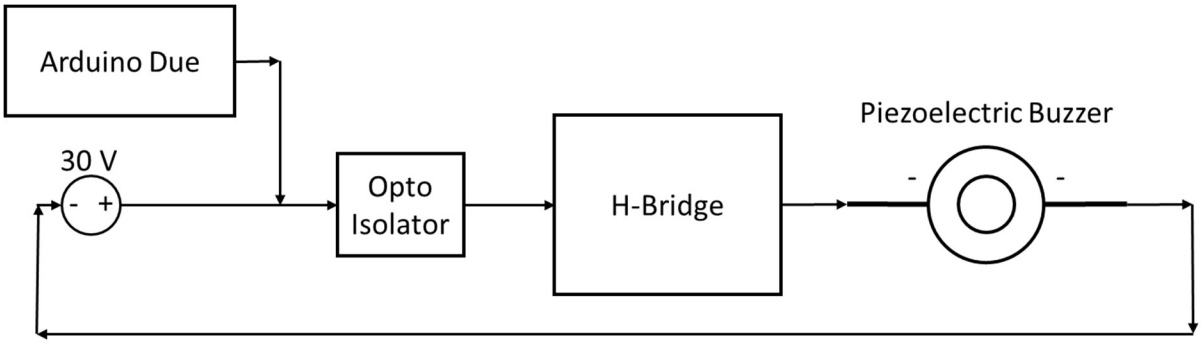

Figure 3-3 Circuit diagram for the piezoelectric droplet on demand generator.

Hydrogel synthesis

Microspheres were synthesized using equimolar concentrations of TMA and CAA using a modified procedure based on previous work from this research group [33]. First, 11.25 mL of 3 M NaOH, 7.5 mL of ethanol, and 11.25 mL of ethylene glycol were combined to make 30 mL of a buffer solution. Then, 36.3 mL of TMA (1.8 M) and 20.2 mL of CAA (1.8 M) were added to the solution and mixed thoroughly. Then, 13.5 mL TEGDMA was used as the cross-linker to create a 6.6:1 monomer to cross-linker ratio (4X cross-linker density). Finally, one of two photoinitiators was added to the solution to initiate the reaction when exposed to UV. LAP and Irgacure 2959 were tested to determine the optimal polymerization conditions. This formulation was selected based on trial and error studies to get the highest concentration of monomer while still being able to produce droplets. At too high of a monomer concentration, the solution properties would not allow for droplet formation. The solutions tested consisted of buffer to monomer ratios shown in Table 3-1. Once the initiator was selected, six different concentrations (0.01, 0.05, 0.1, 0.5, 1.1, and 5% weight/volume) were used to determine which concentration gave the quickest polymerization. This was done externally from the droplet generator using a pipette with 5 and 2.5 µL of polymer solution beaded at the pipet tip and held in the light fixture. Once the optimal concentration was determined, the solution was loaded into the droplet generator and the different nozzles were tested. Three methods of collecting droplets were also tested. First, the droplets fell into a petri dish below the lights. In the second method, the droplets fell in a 100 mL graduated cylinder filled with water below the two light fixtures. For the third collection method, a 15 mL test tube full of water was placed in between the two light fixtures for droplet collection. For all of the results discussed in the following section, the droplet generator ran at 29.4 volts and with a frequency of 20 Hz.

Table 3-1 Different ratios of buffer to monomer tested in the droplet generator.

% Buffer	0	6.7	12.5	24	30
% Monomer & Crosslinker	100	93.3	87.5	76	70

Microsphere characterization

Microsphere sizes were characterized using a Nikon microscope with a 4X and 10X objective. The diameters were measured, and pictures were taken using NIS Elements software. The diameter measurements were taken from 235 droplets from 6-30 samples/picture. Nonfouling tests were conducted to verify that this property was not affected by the synthesis method. For nonfouling testing, microspheres were transferred to a petri dish and they were exposed to 1 mL of 1 mg/mL

FITC-BSA in PBS for 15 minutes. The samples were then rinsed 3 times in neutral PBS to remove unbound protein. Nonfouling was evaluated by comparing the fluorescence of these samples to control samples which were not exposed to protein using an inverted fluorescent Nikon microscope with a 4X objective.

Drug release

Before characterizing the drug release properties of the loaded microsphere, several tests were conducted by measuring the absorbance of color released in solution with a BioTek PowerWave XS2 spectrophotometer. This was done to ensure it was possible to directly detect vitamin D_3 before adding it to the microsphere synthesis process. This was first tested with vitamin D_3 in a solution of PBS and Tween 80 (1% w/v), PBS and sodium dodecyl sulfate (0.1% and 0.5% w/v), or 100% ethanol to improve the solubility [60, 61]. Vitamin D_3 concentrations ranged between 15.6-250 μg/mL. The absorbance was measured at 290 nm to find the minimum detectable level. When it was determined it could not be detected below a concentration of about 125 μg/mL, with the exception of the ethanol solution, an enzyme-linked immunosorbent assay (ELISA) from Aviva Systems Biology was tested. Similar to the first test, vitamin D_3 solutions of 1% SDS in PBS, 1% Tween 80 in PBS, and 1% Tween 80 in Tris buffer were made and then solutions were diluted to a range of concentrations between 1.5 – 200 ng/mL. Procedures from the ELISA kit (OKEH02571) were followed. The absorbance was measured at 450 nm and the wells were compared to the ELISA kit standard. After that, the release properties with metanil yellow loaded microspheres were studied by measuring the absorbance in neutral PBS. Metanil yellow was selected because it is nearly the same size as vitamin D_3 and has demonstrated release with polyampholytes previously [32]. The hydrogels were synthesized with the above method, with the addition of 20 μM metanil yellow. When the test tube was removed from the droplet generator apparatus, the samples were immediately transferred to a 15 mL centrifuge tube and centrifuged at 2500 rpm for 3 minutes. The supernatant was pipetted off the droplets and 3 mL buffer solution was added to the centrifuge tube. To rinse away any polymer solution, it was centrifuged again with the same parameters, and the buffer was removed. This was repeated once more. Finally, 1 mL of buffer was added to the centrifuge tubes as a release media. Samples of the buffer were measured in a 96 well-plate and the absorbance was measured at 430 nm with the plate reader. The buffer was removed and replaced after each measurement was taken.

Results

Droplet Generator

The droplet generator has adjustable parameters including the voltage and the frequency. If the droplet generator ran below 27 volts, droplets would not form with the polymer solution. To keep things consistent, the droplet generator was set to 29.5 volts for all of the trials. Several different frequencies were tested. Below 20 Hz, the polymer solution would polymerize in the nozzle quickly, clogging the system. Above 30 Hz, the droplet generator produced a spray, so droplets were not collected at that setting. Therefore, a frequency of 20 Hz gave the most consistent results. The light intensity was measured when the new light system was added and 2 months after that. The first measurements read between 11.5-13.6 mW/cm^2 when pointing the solarmeter into the light fixture and decreased to 9-11.5 mW/cm^2 after several months of operation.

Hydrogel synthesis

Two photoinitiators and the initiator concentration were tested to determine what would give the quickest polymerization. Even at high concentrations, Irgacure 2959 had a slow polymerization time. As a result, no droplets were collected because they did not form by the time they landed in the collection vessel. LAP was much more successful in forming polymer microspheres due to faster kinetics [62]. In order to determine the best concentration, six different concentrations were used and the time to polymerize was measured. The results are summarized in Table 3-2. At a concentration of 0.5% weight/volume, the polymerization time was under 2 seconds on average, whereas all the other concentrations tested resulted in polymerization times upwards of 2 seconds.

Table 3-2 Average time for droplets to polymerize based on concentration of photoinitiator

Polymerization Kinetics						
LAP Concentration (% w/v)	0.01	0.07	0.1	0.5	1.1	5
Average Time (s)	8.03	6.06	2.65	1.55	2.11	3.28
Standard Deviation	1.40	1.69	0.51	0.23	0.20	0.65

Of the three nozzles tested, the 0.4 and 0.6 mm nozzles consistently had wicking issues that prevented droplet formation. The 1 mm nozzle would have wicking issues, but it did not prevent droplet generation. It was found that thoroughly cleaning the nozzle would often avert fluid wicking up the nozzle. This was done by clearing the inside and outside of the nozzle to remove any polymer residue.

Of the three collection methods tested, droplet formation would occur for only the test tube and graduated cylinder methods. The water helped slow the droplet down to increase the degree of

polymerization, by increasing the light exposure time. Both methods had issues with a polymer film forming on top of the water that would sometimes prevent droplet collection. This was more prevalent with the test tube method due to the small diameter and reduced level of light exposure. More of the polymer solution was wasted because it hit water before much light exposure took place and had a much smaller fall distance (17cm) than the graduated cylinder (41 cm). Less droplets were collected with the graduated cylinder method likely because it was not slowed down initially while falling through the light fixtures. Based on these results, LAP with a 0.5% weight/volume concentration, the 1 mm nozzle, and the test tube method were used for all subsequent studies.

Microsphere characterization

The microsphere size distribution is shown in Figure 3-4. It shows there was large variation of microsphere sizes ranging from under 4 μm up to 450 μm. The distribution shows an exponential decrease, as the droplets get larger. Microspheres under 4 μm in diameter were not quantified due to the large number of microspheres above this size range. Figure 3-5 gives a visual of the size distribution. Both images were taken from samples in the same experimental run, with a 4X objective.

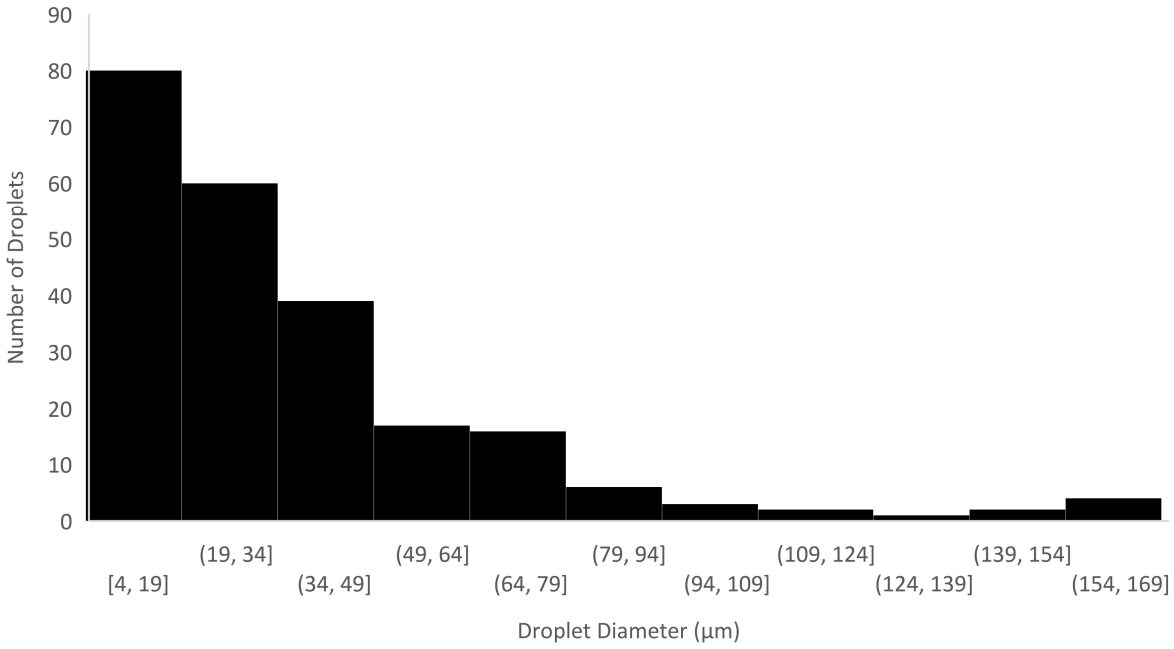

Figure 3-4 Size distribution of droplets.

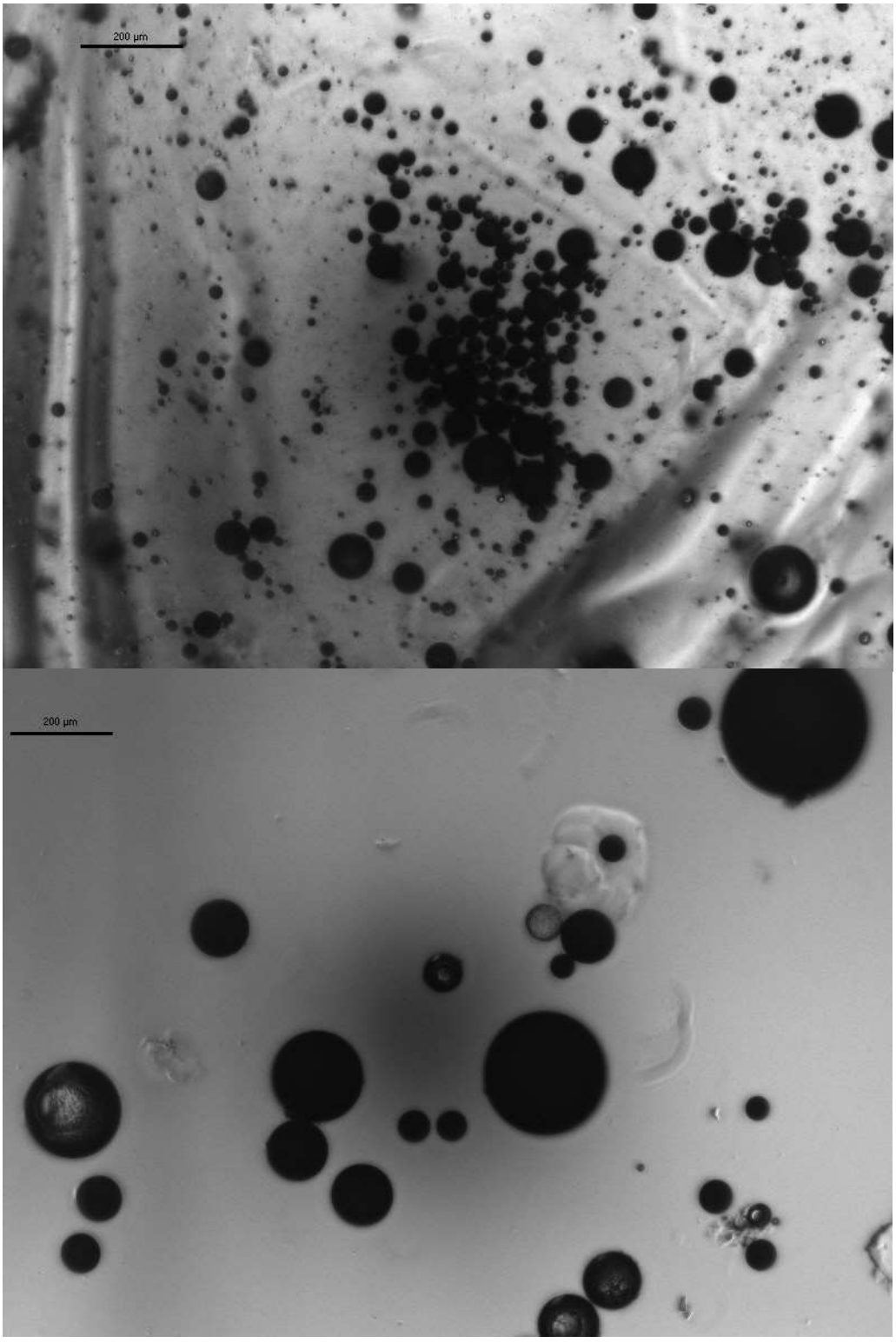

Figure 3-5 Representative light microscopy images (4X) highlighting the range of polyampholyte microspheres obtained from the droplet generator..

One key feature for the intended application is nonfouling and this was assessed using FITC-BSA and fluorescent microscopy. Representative microscopy images highlighting the nonfouling property are shown in Figure 3-6. The circled droplet is the nonfouling microsphere that was exposed to protein, while the others are controls that were not exposed to FITC-BSA. There is no visible fluorescence on the circled droplet relative to the unexposed controls, demonstrating that the droplet generation procedure and modified polymer solution does not affect the known nonfouling capabilities.

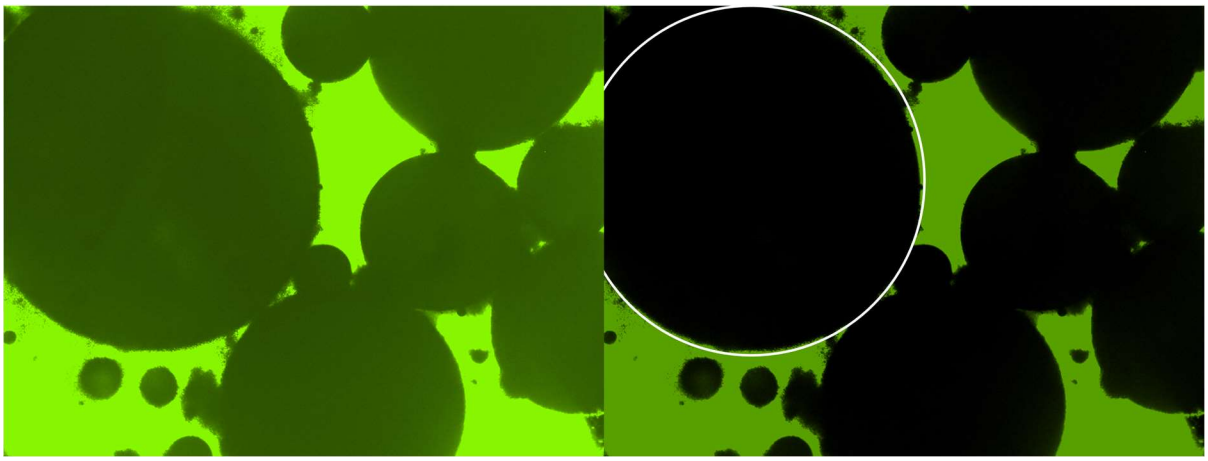

Figure 3-6 Representative fluorescent microscopy images following FITC-BSA adsorption. The circled droplet was exposed to FITC-BSA and the rest are control microspheres.

Drug release

The vitamin D_3 tests that were conducted were unsuccessful. This is likely due to the poor solubility of vitamin D_3 in PBS, even with the addition of a surfactant. Figure 3-7 shows the direct detection absorbance profiles of vitamin D_3 in different solutions. There was some degree of detection at higher concentrations, but it was not expected that the microspheres would release vitamin D at that high of a concentration level. Additionally, with the poor solubility, it was unlikely there would be release into any PBS [60]. Therefore, the direct detection of vitamin D_3 is not viable using absorbance.

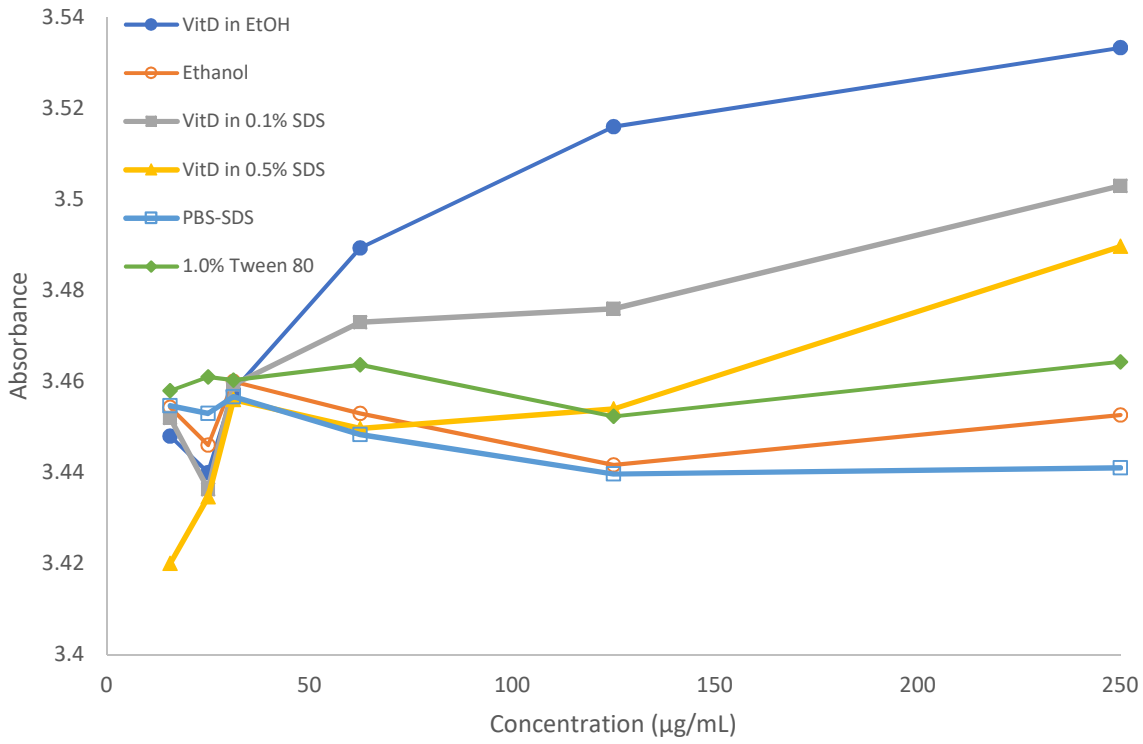

Figure 3-7 Absorbance of vitamin D_3 in different solutions

Because direct detection of vitamin D_3 was not possible at the relevant concentration levels, indirect detection was pursued with a commercially available ELISA kit. However, concentration differences of vitamin D_3 were not detected with the ELISA kit. Again, this was likely due to poor solubility. Figure 3-8 shows the ELISA results for vitamin D_3 in different buffers. The standard curve matched the curve in the kit instructions and was to be used to determine the concentrations of vitamin D_3 in the solution. However, in each of the laboratory control samples, it is readily apparent that there is no significant signal change with varying concentrations. It was concluded that these results do not give an accurate measurement of the vitamin D_3 concentrations. Further research must be done on vitamin D delivery systems to use polyampholytes for this application.

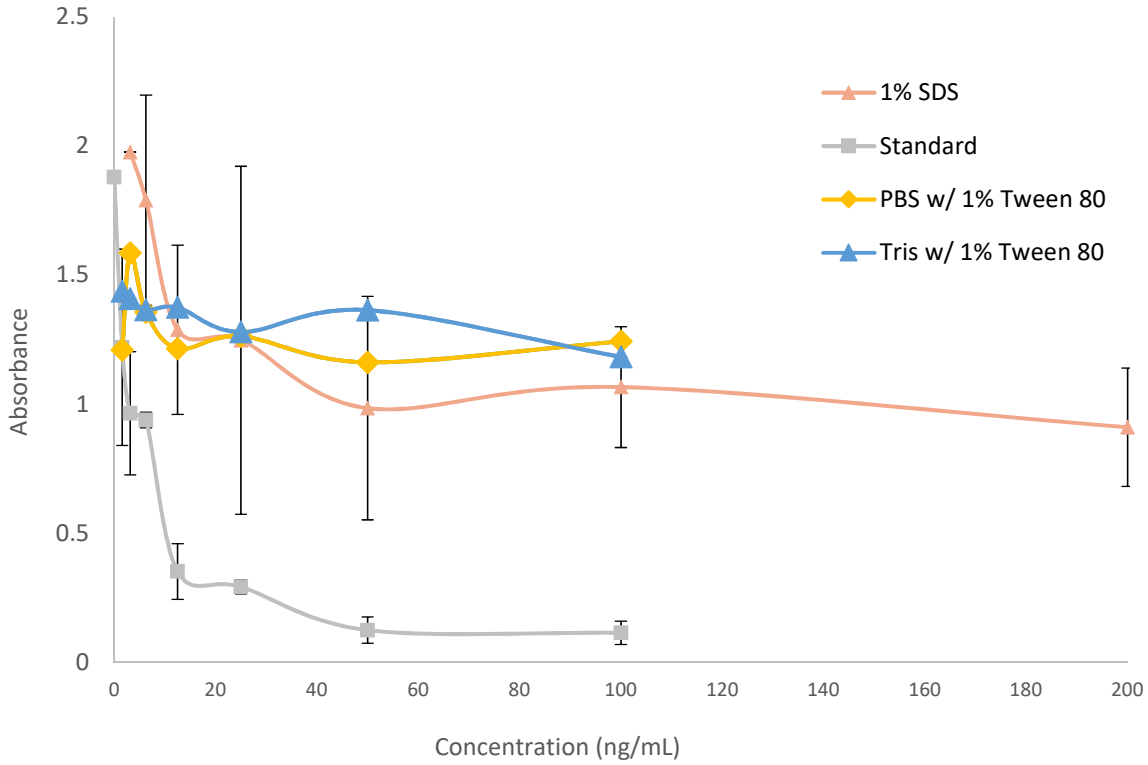

Figure 3-8 ELISA test curves.

Because vitamin D_3 was not detectable through either direct or indirect approaches, metanil yellow tests were conducted instead. The release of metanil yellow was evaluated over a 98-hour period. The averaged results of this study can be seen in Figure 3-9. There was a large amount of error generated due to inconstant amounts of droplets in each evaluation sample, large variation in microsphere size, and loss of metanil yellow during the multiple rinse cycles. Overall, this experiment was also unsuccessful at demonstration long-term controlled release, but it did demonstrate short-term release from the polyampholyte microspheres.

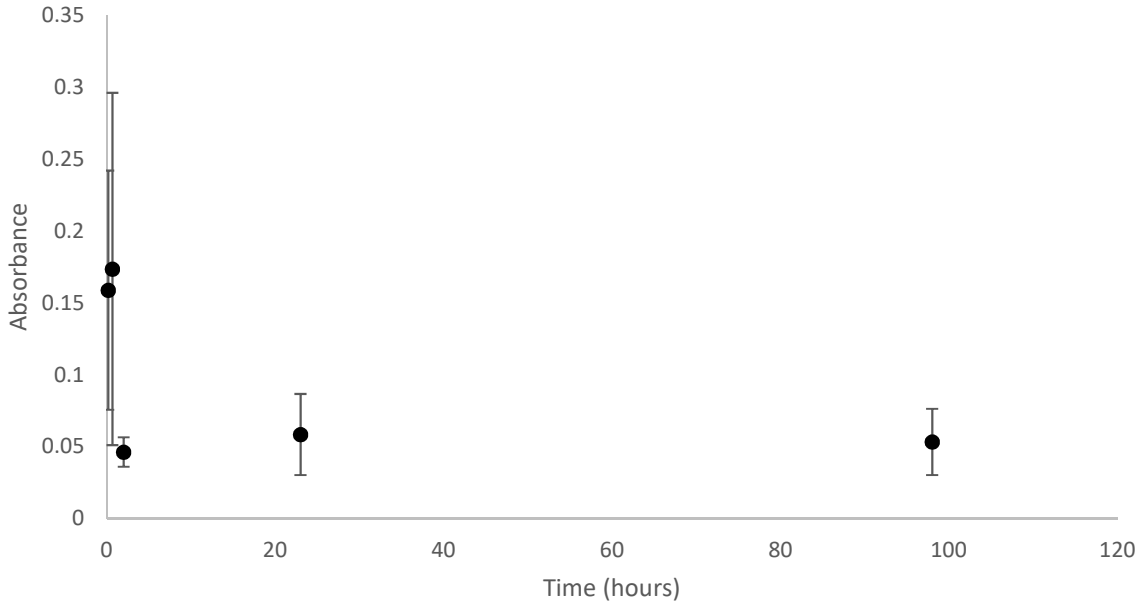

Figure 3-9 Metanil yellow drug release profile.

Discussion

Several different ratios of monomer to buffer were tested before settling on the formula discussed in the methods section. This was done to determine how much monomer/cross-linker could be used before droplets no longer formed. A higher concentration of monomer and cross-linker was desired to speed up polymerization. The ratio used worked well for the 1 mm nozzle but polymer droplets would not form with the 0.4 - 0.6 mm nozzle. Instead, solution wicked up the side of the nozzle. This issue was prevalent in the experiments conducted by Hudson et al. [59]. They believed the piezo pulse was not strong enough to separate a droplet from the bulk solution, and the repeated pulsing of fluid without ejection resulted in wicking due to the surface tension of the polymer solution [59]. Droplets would form with the 0.6 mm nozzle when the system ran with water, demonstrating the wicking could be a result of the polymer solution properties. Harris et al. used nozzles with diameters between 0.5-1.4 mm [58]. They used the Ohnesorge number (Oh) to determine the influence of viscous and capillary forces shown by Equation 3-1.

$$Oh = \frac{\mu}{\sqrt{\sigma R_n \rho}} \tag{3-1}$$

Here, μ, σ, R_n, and ρ are the dynamic viscosity, surface tension, nozzle radius, and density, respectively. Harris et al. used silicone oil in their study and found Oh values between 0.16 -0.28 [58]. It could be worth determining Oh to see if it is in range of their values because they expected their system would work best with viscosities the same as or lower than silicone oil [58]. To calculate this, the dynamic viscosity, surface tension, and density of the polymer solution are needed.

As discussed in the methods, two photoinitiators were tested. Irgacure 2959 had a slow polymerization time, so there was little success in droplet generation. LAP has become more common in use for biomedical applications because it is noncytotoxic and has a peak absorbance at 375 nm [62]. It was determined that LAP was more suitable for this study because it has good overlap with the emission wavelength of the LEDs used in this experiment (365 nm) and polymerized more quickly than Irgacure 2959. The decrease in UV intensity over the lifetime of these studies could have had an effect on the photopolymerization over time. UV is what generates the radicals for polymerization, so less intense lights would result in less radicals being generated. That could slow down the bulk polymerization kinetics and should be evaluated further if updates are made on the droplet generator system.

Although the test tube method of collection wasted more solution, it created a wide range of droplets sizes, with many under 5 μm. Injectable microspheres must be smaller than 6 μm so they will not block the capillaries, and in some cases, smaller than 100 nm [13]. Given the size distribution of the microspheres synthesized in this study, they could be used for this method of delivery if they are further separated by size. This could be done by micro sieving or centrifugation. It might be better to get more complete polymerization in order to avoid wasted solution and for use in other applications that do not require injection into the bloodstream. Methods to slow down the droplets and adding more LEDs could help. This could be done by dropping the spheres into different, more viscous media as long as it does not further alternate the light intensity. If more complete polymerization is obtained, that could give sizes that are more consistent. It could also reduce the need for a rinsing step after droplet collection. Mixing droplet sizes can also be used to control release rates due to the different release properties, as size is one parameter that controls release [13, 42]. Smaller droplets have faster release properties than larger ones where it takes more time for the drugs to diffuse out and is partially dependent on degradation of the loaded microspheres [13, 42]. This was demonstrated by the rapid release of metanil yellow in this study.

Other ways to improve the system would be to update the mount to fit additional lights and a fluid-filled collection chamber. Additionally, adding a hydrophobic coating on the nozzle could also help. The nozzle had to be wiped too frequently due to wicking. This wastes the solution and disrupts the generator while running, as droplets do not eject. While adjusting the reservoir height and cleaning the nozzle and generator often help mitigate this issue, it still occurs frequently while running. These adjustments will help the system run more consistently without interruption so other parameters can be adjusted to influence droplet size, such as the voltage supplied to the piezo.

Conclusion

In this study, microspheres were successfully generated with a custom-built droplet on demand generator. Microspheres ranged in sizes between 1 and 450 μm. The nonfouling studies confirmed that the polyampholyte microspheres do not adsorb protein. While aspects of this project were very successful, drug release studies were not effective. Of the three tests conducted, none of them showed potential for quantifying release properties of vitamin D_3 or long-term release of metanil yellow. If this were tested again, it would be best to make the suggested changes on the droplet generator to obtain more complete polymerization. That would eliminate the need for rinse steps, which was one factor that affected the ability to quantify release.

Chapter 4: Conclusion

This work aimed to assess the tunability of polyampholyte polymers for their use in tissue engineering and drug delivery applications. This was explored in two separate projects. The first, exploring the physical and mechanical properties of polyampholyte hydrogels with cross-linkers of different chain lengths. The second, identifying light-initiated polymerization procedures to develop microdroplet polymers for drug delivery using a custom built droplet on demand generator. Previous work has shown that these polymers can be tuned based on monomer composition and cross-linker density. Several tunable parameters include biomolecule release rate, mechanical strength, and swelling capacity. They have nonfouling properties and conjugation capabilities that are not dependent on the composition, which make them very suitable for biomedical applications.

This work shows that polyampholytes can further be tuned with cross-linker choice. This is most evident with the degradation studies where it demonstrated that cross-linker choice determines the degradation pathway. The Tetra-EGDMA samples degraded in bulk, which potentially makes them less suitable for use as a tissue engineered scaffold considering they swelled in size and broke apart all at once. DEGDMA and TEGDMA took a surface degradation pathway. Surface degradation is more suitable for tissue engineering applications because it could maintain support as new tissue forms.

The compression testing demonstrated that these hydrogels could only be strained so much before they shattered, regardless of the cross-linker density. This is likely due to their high water content and water is incompressible. Additionally, the magnitude of change in the mechanical properties as cross-linker density increased was found to be more dependent on the species rather than how much additional cross-linker is in the hydrogel. Further research must be done to understand the behavior of these hydrogels as cross-linker changes. One suggestion on understanding these properties better would be to study the hydrogels with different ratios of monomer and solvent.

The tunable release properties of polyampholyte microspheres could not be quantified with the current droplet generator system. While the nonfouling properties were verified with the microspheres, there was too much variability in the samples collected to use the system as is. Drug release studies with Vitamin D_3 were not successful and only short-term release with metanil yellow was demonstrated. The droplet on demand generator must be improved to use the microspheres as drug delivery vehicles.

Updating the mount could help give results that are more consistent because the reservoir could be attached to the micrometer translation stage and adjusted more easily. This could help

prevent some of the wicking issues that were very prevalent during droplet generation. Extra lights should be added to the system to improve polymerization. Additionally, developing a different collection method could prevent issues that occurred when the droplets fell into water, including solution waste and polymerization occurring on the surface of the water. These steps could reduce variability in droplet size, decrease solution waste, and remove the need for multiple rinsing steps. A potential new system would be to have the collection tube full of water below one set of lights to initiate polymerization before it reaches the water. Two additional light fixtures surrounding the collection vessel could be added to ensure polymerization is still occurring as the droplets fall.

There is still a lot of work to be done before polyampholytes can be used as tissue engineered scaffolds. While these polymers show a lot of promise with their multifunctionality and tunable capabilities, there is still a need to learn more about the tunable parameters so they can be used for targeted applications. Additionally, they will need to be tested in vivo to understand how they will behave in that environment. The ability for these hydrogels to be used for drug delivery has been demonstrated. Therefore, polyampholyte microspheres show promise for use as a drug delivery vehicle if the issues with the droplet on demand generator are addressed.

Literature Cited

1. Slaughter, B.V., et al., *Hydrogels in Regenerative Medicine.* Advanced Materials, 2009. **21**(32-33): p. 3307-3329.
2. Zhang, L., et al., *Zwitterionic hydrogels implanted in mice resist the foreign-body reaction.* Nature Biotechnology, 2013. **31**: p. 553.
3. Anderson, J.M., A. Rodriguez, and D.T. Chang, *Foreign body reaction to biomaterials.* Seminars in immunology, 2008. **20**(2): p. 86-100.
4. Nair, L.S. and C.T. Laurencin, *Biodegradable polymers as biomaterials.* Progress in Polymer Science, 2007. **32**(8): p. 762-798.
5. Saroia, J., et al., *A review on biocompatibility nature of hydrogels with 3D printing techniques, tissue engineering application and its future prospective.* Bio-Design and Manufacturing, 2018. **1**(4): p. 265-279.
6. Li, X., et al., *Functional Hydrogels With Tunable Structures and Properties for Tissue Engineering Applications.* Frontiers in Chemistry, 2018. **6**(499).
7. Hutmacher, D.W., *Scaffolds in tissue engineering bone and cartilage.* Biomaterials, 2000. **21**(24): p. 2529-2543.
8. Rice, M.A. and K.S. Anseth, *Encapsulating chondrocytes in copolymer gels: Bimodal degradation kinetics influence cell phenotype and extracellular matrix development.* Journal of Biomedical Materials Research Part A, 2004. **70A**(4): p. 560-568.
9. Hassanzadeh, P., et al., *Ultrastrong and Flexible Hybrid Hydrogels based on Solution Self-Assembly of Chitin Nanofibers in Gelatin Methacryloyl (GelMA).* Journal of materials chemistry. B, 2016. **4**(15): p. 2539-2543.
10. Chan, B.P. and K.W. Leong, *Scaffolding in tissue engineering: general approaches and tissue-specific considerations.* European spine journal : official publication of the European Spine Society, the European Spinal Deformity Society, and the European Section of the Cervical Spine Research Society, 2008. **17 Suppl 4**(Suppl 4): p. 467-479.
11. Discher, D.E., P. Janmey, and Y.-l. Wang, *Tissue Cells Feel and Respond to the Stiffness of Their Substrate.* Science, 2005. **310**(5751): p. 1139-1143.
12. Wechsler, M.E., et al., *Engineered microscale hydrogels for drug delivery, cell therapy, and sequencing.* Biomedical Microdevices, 2019. **21**(2): p. 31.
13. Freiberg, S. and X.X. Zhu, *Polymer microspheres for controlled drug release.* International Journal of Pharmaceutics, 2004. **282**(1): p. 1-18.
14. Narayanaswamy, R. and V.P. Torchilin, *Hydrogels and Their Applications in Targeted Drug Delivery.* Molecules, 2019. **24**(3): p. 603.
15. Saini, S., et al., *MICROSPHERES AS CONTROLLED DRUG DELIVERY SYSTEM: AN UPDATED REVIEW.* International Journal of Pharmaceutical Sciences and Research, 2018. **9**: p. 1760+.
16. Tyler, B., et al., *Polylactic acid (PLA) controlled delivery carriers for biomedical applications.* Advanced Drug Delivery Reviews, 2016. **107**: p. 163-175.
17. Nguyen, K.T. and J.L. West, *Photopolymerizable hydrogels for tissue engineering applications.* Biomaterials, 2002. **23**(22): p. 4307-4314.
18. Munim, S.A. and Z.A. Raza, *Poly(lactic acid) based hydrogels: formation, characteristics and biomedical applications.* Journal of Porous Materials, 2018.
19. Gyles, D.A., et al., *A review of the designs and prominent biomedical advances of natural and synthetic hydrogel formulations.* European Polymer Journal, 2017. **88**: p. 373-392.

20. Korzhikov-Vlakh, V., et al., *Hydrogel Layers on the Surface of Polyester-Based Materials for Improvement of Their Biointeractions and Controlled Release of Proteins.* Polymers, 2016. **8**(12): p. 418.
21. Rasal, R.M., A.V. Janorkar, and D.E. Hirt, *Poly(lactic acid) modifications.* Progress in Polymer Science, 2010. **35**(3): p. 338-356.
22. Khampieng, T., et al., *Protein adsorption and cell behaviors on polycaprolactone film: The effect of surface topography.* Advances in Polymer Technology, 2018. **37**(6): p. 2030-2042.
23. Zhu, Y., et al., *Surface Modification of Polycaprolactone Membrane via Aminolysis and Biomacromolecule Immobilization for Promoting Cytocompatibility of Human Endothelial Cells.* Biomacromolecules, 2002. **3**(6): p. 1312-1319.
24. Lingyan, L., C. Shengfu, and J. Shaoyi, *Protein interactions with oligo(ethylene glycol) (OEG) self-assembled monolayers: OEG stability, surface packing density and protein adsorption.* Journal of Biomaterials Science -- Polymer Edition, 2007. **18**(11): p. 1415-1427.
25. Zheng, L., et al., *Applications of zwitterionic polymers.* Reactive and Functional Polymers, 2017. **118**: p. 51-61.
26. Tagami, T., et al., *Anti-PEG IgM production by siRNA encapsulated in a PEGylated lipid nanocarrier is dependent on the sequence of the siRNA.* Journal of Controlled Release, 2011. **151**(2): p. 149-154.
27. Cao, B., Q. Tang, and G. Cheng, *Recent advances of zwitterionic carboxybetaine materials and their derivatives.* Journal of Biomaterials Science -- Polymer Edition, 2014. **25**(14/15): p. 1502-1513.
28. Bernards, M. and Y. He, *Polyampholyte polymers as a versatile zwitterionic biomaterial platform.* Journal of Biomaterials Science -- Polymer Edition, 2014. **25**(14/15): p. 1479-1488.
29. Ji, Y., et al., *Zwitterionic polycarboxybetaine coating functionalized with REDV peptide to improve selectivity for endothelial cells.* Journal of Biomedical Materials Research Part A, 2012. **100A**(6): p. 1387-1397.
30. Wang, J. and N. Hui, *Zwitterionic poly(carboxybetaine) functionalized conducting polymer polyaniline nanowires for the electrochemical detection of carcinoembryonic antigen in undiluted blood serum.* Bioelectrochemistry, 2019. **125**: p. 90-96.
31. Carr, L., et al., *Engineering the Polymer Backbone To Strengthen Nonfouling Sulfobetaine Hydrogels.* Langmuir, 2010. **26**(18): p. 14793-14798.
32. Barcellona, M.N., N. Johnson, and M.T. Bernards, *Characterizing Drug Release from Nonfouling Polyampholyte Hydrogels.* Langmuir, 2015. **31**(49): p. 13402-13409.
33. Schroeder, M.E., et al., *Multifunctional Polyampholyte Hydrogels with Fouling Resistance and Protein Conjugation Capacity.* Biomacromolecules, 2013. **14**(9): p. 3112-3122.
34. Haag, S.L. and M.T. Bernards, *Polyampholyte Hydrogels in Biomedical Applications.* Gels, 2017. **3**(4): p. 41.
35. Bernards, M.T., et al., *Nonfouling Polymer Brushes via Surface-Initiated, Two-Component Atom Transfer Radical Polymerization.* Macromolecules, 2008. **41**(12): p. 4216-4219.
36. Cao, S., et al., *Tunable multifunctional tissue engineering scaffolds composed of three-component polyampholyte polymers.* Journal of Applied Polymer Science, 2016. **133**(40).
37. Dobbins, S.C., D.E. McGrath, and M.T. Bernards, *Nonfouling Hydrogels Formed from Charged Monomer Subunits.* The Journal of Physical Chemistry B, 2012. **116**(49): p. 14346-14352.
38. Raveling, A.R., S.K. Theodossiou, and N.R. Schiele, *A 3D printed mechanical bioreactor for investigating mechanobiology and soft tissue mechanics.* MethodsX, 2018. **5**: p. 924-932.
39. Ikeda-Fukazawa, T., et al., *Effects of crosslinker density on the polymer network structure in poly-N,N-dimethylacrylamide hydrogels.* Journal of Polymer Science Part B: Polymer Physics, 2013. **51**(13): p. 1017-1027.

40. Burkersroda, F.v., L. Schedl, and A. Göpferich, *Why degradable polymers undergo surface erosion or bulk erosion.* Biomaterials, 2002. **23**(21): p. 4221-4231.
41. Ulery, B.D., L.S. Nair, and C.T. Laurencin, *Biomedical applications of biodegradable polymers.* Journal of Polymer Science Part B: Polymer Physics, 2011. **49**(12): p. 832-864.
42. Saralidze, K., L.H. Koole, and M.L.W. Knetsch, *Polymeric Microspheres for Medical Applications.* Materials, 2010. **3**(6): p. 3537-3564.
43. Shi, L.B., et al., *Tissue engineered bulking agent with adipose-derived stem cells and silk fibroin microspheres for the treatment of intrinsic urethral sphincter deficiency.* Biomaterials, 2014. **35**(5): p. 1519-1530.
44. Lemperle, G., et al., *Urethral Bulking With Polymethylmethacrylate Microspheres for Stress Urinary Incontinence: Tissue Persistence and Safety Studies in Miniswine.* Urology, 2011. **77**(4): p. 1005.e1-1005.e7.
45. Patel, R., et al., *Polymeric microspheres: a delivery system for osteogenic differentiation.* Polymers for Advanced Technologies, 2017. **28**(12): p. 1595-1609.
46. Ray, P., et al., *Size-Transformable, Multifunctional Nanoparticles from Hyperbranched Polymers for Environment-Specific Therapeutic Delivery.* ACS Biomaterials Science & Engineering, 2019. **5**(3): p. 1354-1365.
47. Berkland, C., K. Kim, and D.W. Pack, *PLG Microsphere Size Controls Drug Release Rate Through Several Competing Factors.* Pharmaceutical Research, 2003. **20**(7): p. 1055-1062.
48. Bezemer, J.M., et al., *Microspheres for protein delivery prepared from amphiphilic multiblock copolymers: 1. Influence of preparation techniques on particle characteristics and protein delivery.* Journal of Controlled Release, 2000. **67**(2): p. 233-248.
49. Pouton, C.W. and L.W. Seymour, *Key issues in non-viral gene delivery.* Advanced Drug Delivery Reviews, 1998. **34**(1): p. 3-19.
50. Zha, L., B. Banik, and F. Alexis, *Stimulus responsive nanogels for drug delivery.* Soft Matter, 2011. **7**(13): p. 5908-5916.
51. Morelli, S., R.G. Holdich, and M.M. Dragosavac, *Chitosan and Poly (Vinyl Alcohol) microparticles produced by membrane emulsification for encapsulation and pH controlled release.* Chemical Engineering Journal, 2016. **288**: p. 451-460.
52. Nista, E.C., et al., *Bacillus clausii therapy to reduce side-effects of anti-Helicobacter pylori treatment: randomized, double-blind, placebo controlled trial.* Alimentary Pharmacology & Therapeutics, 2004. **20**(10): p. 1181-1188.
53. Wang, Z., et al., *Development of Zwitterionic Polymer-Based Doxorubicin Conjugates: Tuning the Surface Charge To Prolong the Circulation and Reduce Toxicity.* Langmuir, 2014. **30**(13): p. 3764-3774.
54. Smith, S.M., et al., *Space Flight Calcium: Implications for Astronaut Health, Spacecraft Operations, and Earth.* Nutrients, 2012. **4**(12): p. 2047-2068.
55. Smith, S.M., et al., *Vitamin D supplementation during Antarctic winter.* The American Journal of Clinical Nutrition, 2009. **89**(4): p. 1092-1098.
56. Bikle, D., *Nonclassic Actions of Vitamin D.* The Journal of Clinical Endocrinology & Metabolism, 2009. **94**(1): p. 26-34.
57. Holick, M.F., *Vitamin D: importance in the prevention of cancers, type 1 diabetes, heart disease, and osteoporosis.* The American Journal of Clinical Nutrition, 2004. **79**(3): p. 362-371.
58. Harris, D.M., T. Liu, and J.W.M. Bush, *A low-cost, precise piezoelectric droplet-on-demand generator.* Experiments in Fluids, 2015. **56**(4): p. 83.
59. Hudson, C., et al., *Drug Delivery Capsules* in *Chemical and Materials Engineering*. 2018, University of Idaho.

60. Ramezanli, T., et al., *Polymeric nanospheres for topical delivery of vitamin D3.* International Journal of Pharmaceutics, 2017. **516**(1): p. 196-203.
61. Bile, J., et al., *The parameters influencing the morphology of poly(ε-caprolactone) microspheres and the resulting release of encapsulated drugs.* International Journal of Pharmaceutics, 2015. **494**(1): p. 152-166.
62. Fairbanks, B.D., et al., *Photoinitiated polymerization of PEG-diacrylate with lithium phenyl-2,4,6-trimethylbenzoylphosphinate: polymerization rate and cytocompatibility.* Biomaterials, 2009. **30**(35): p. 6702-6707.